NAA-SR-5417
REACTORS-GENERAL &
REACTOR SAFETY
54 PAGES

KINETIC EXPERIMENTS ON WATER BOILERS

- "A" CORE REPORT -

PART III - PILE OSCILLATOR RESULTS

By
R. N. CORDY

ATOMICS INTERNATIONAL

A DIVISION OF NORTH AMERICAN AVIATION, INC.
P.O. BOX 309 CANOGA PARK, CALIFORNIA

CONTRACT: AT(11-1)-GEN-8
ISSUED: DEC 1 1960

DISCLAIMER

DISTRIBUTION

This report has been distributed according to the category "Reactors-General" as given in "Standard Distribution Lists for Unclassified Scientific and Technical Reports" TID-4500 (15th Ed.), August 1, 1959, and special distribution for Reactor Safety Reports (see list UC-80). A total of 725 copies was printed.

ACKNOWLEDGMENT

The author is indebted to many people for their cooperation during all phases of this study, and would specifically like to express his gratitude to John W. Flora for his encouragement, in addition to his many helpful suggestions; to Edward L. Gardner for his excellent instrumentation designs which well satisfied the strict limitations of this experiment; and to the KEWB operation crew for their unusually fine assistance in all operating aspects of the reactor.

CONTENTS

TABLES

FIGURES

FIGURES

PREFACE

This is Part III in a series of five reports concerning the developments which occurred during the first ("A" Core) phase of the Kinetic Experiments on Water Boilers (KEWB) program. The reader will undoubtedly find other reports in the series helpful if he is interested in further details of the KEWB program. These reports, which are in final preparation, are designated as:

NAA-SR-5415, J. W. Flora, ed., "Kinetic Experiments on Water Boilers - "A" Core Report - Part I - Program History, Facility Description, and Experimental Results."

NAA-SR-5416, M. S. Dunenfeld, et al., "Kinetic Experiments on Water Boilers - "A" Core Report - Part II - Analysis of Results."

NAA-SR-5418, M. A. Greenfield, "Kinetic Experiments on Water Boilers - "A" Core Report - Part IV - Containment Aspects of Hydrogen Oxygen Explosions."

NAA-SR-5419, M. A. Greenfield, "Kinetic Experiments on Water Boilers - "A" Core Report - Part V - Containment Aspects of Pressure Waves from Initial Solution Expansion."

ABSTRACT

A brief review of the theoretical water boiler reactor power transfer function is presented as background for the experimental determination of the ratio of effective prompt neutron lifetime to the effective fraction of delayed neutrons, ℓ/β. The preparation and performance of the experiment are discussed with special emphasis on equipment, procedures, and measurement errors. The results, which strongly support a seven delay group model of the reactor, are presented and compared with theoretical six and seven group models. The experiment indicates qualitative values of the seventh group constants, and it also indicates an $\ell/\beta = 7.7 \pm .3$ milliseconds valid for all but short period transients.

I. OBJECTIVE

An analysis of transient experiments has indicated that the performance of the KEWB reactor is not adequately described by the conventional reactor kinetics model using six groups of delayed neutrons. This reactor modulation experiment was performed in order to resolve this anomaly and to obtain an independent determination of the ratio of prompt neutron lifetime to the effective fraction of delayed neutrons.

II. THE THEORETICAL REACTOR TRANSFER FUNCTION

A. GENERAL THEORY

The transfer function for a water boiler reactor, which is described by the following system of linear and nonlinear space independent kinetics equations, has been determined by Skinner and Hetrick.[1] (The nomenclature for these and subsequent equations is given on page 45.)

$$\frac{dP(t)}{dt} + \frac{\beta - \rho(t)}{\ell} P(t) - \sum_{j=1}^{m} \lambda_j C_j(t) = 0 \qquad \ldots(1)$$

$$\frac{dC_j(t)}{dt} + \lambda_j C_j(t) = \frac{\beta a_j}{\ell} P(t), \qquad (j = 1, 2, \ldots m) \qquad \ldots(2)$$

$$\frac{dT(t)}{dt} + \gamma T(t) = K \left[P(t) - P_0\right] \qquad \ldots(3)$$

$$\frac{dV(t)}{dt} + \sigma V(t) = G \left[P(t) - P_0\right] \qquad \ldots(4)$$

$$\rho(t) = \rho_1(t) + \alpha T(t) + \phi V(t) \qquad \ldots(5)$$

The general expression for the transfer function, of the physical system described by the solution to the linearized form of these equations, can be written

as the ratio of the Fourier transform of the output to the same transform of the input forcing function, i.e.,

$$G_{\bar{p}}(i\omega;P_0) = \frac{\mathcal{F}\left[\delta P_1(t);i\omega\right]}{\mathcal{F}\left[\rho_1(t);i\omega\right]} . \qquad \ldots(6)$$

The transfer function can be normalized to the average reactor power provided reactivity is expressed in dollars;* specifically,

$$G_p(i\omega;P_0) = \frac{\beta}{P_0} G_{\bar{p}}(i\omega;P_0). \qquad \ldots(7)$$

The kinetic equations are linearized for $\frac{\delta P_1}{P_0} << 1$ and the normalized power transfer function is obtained as

$$G_p(i\omega;P_0) = \left[i\omega\ell^* + i\omega \sum_{j=1}^{m} \frac{a_j}{i\omega + \lambda_j} - \frac{\alpha^* K P_0}{i\omega + \gamma} - \frac{\phi^* G P_0}{i\omega + \sigma} \right]^{-1} . \qquad \ldots(8)$$

The transfer function for a stable linear system can be written as

$$G_p(i\omega;P_0) = \left[A_1^2 + A_2^2\right]^{-1/2} \exp\left[i\theta(i\omega;P_0)\right], \qquad \ldots(9)$$

for the case of forced oscillation of the form $\rho_1(t) = \rho_0 \exp(i\omega t)$.

By equating Equations 8 and 9 and by separating the real and imaginary portions, the following values are obtained:

*A reactor has a reactivity of one dollar when at prompt critical; i.e. reactivity in dollars $\equiv \frac{k_{ex}}{\beta}$.

$$A_1(i\omega;P_0) = \left[\sum_{j=1}^{m} \frac{a_j\omega^2}{\omega^2 + \lambda_j^2} - \frac{\gamma K\alpha^* P_0}{\omega^2 + \gamma^2} - \frac{\sigma G\phi^* P_0}{\omega^2 + \sigma^2}\right] \quad \ldots(10)$$

$$A_2(i\omega;P_0) = \left[\ell^* + \sum_{j=1}^{m} \frac{a_j\lambda_j}{\omega^2 + \lambda_j^2} + \frac{K\alpha^* P_0}{\omega^2 + \gamma^2} + \frac{G\phi^* P_0}{\omega^2 + \sigma^2}\right] \quad \ldots(11)$$

$$\theta(i\omega;P_0) = \arctan\left(-\frac{A_2}{A_1}\right) \quad \ldots(12)$$

The transfer function of a water boiler can now be described by amplitude and phase equations; where

$$\left|G_p(i\omega;P_0)\right| = \left[A_1^2 + A_2^2\right]^{-1/2} \quad \ldots(13)$$

and where

$$\angle G_p(i\omega;P_0) = \arctan\left(-\frac{A_2}{A_1}\right) \quad \ldots(14)$$

The transfer function for a six group model of the KEWB reactor, as computed from Equations 13 and 14, is presented in Figures 1 and 2. The values used in these calculations are given in Tables I and II.

Transient experimentation has indicated that a six delay group model does not adequately describe the operation of the KEWB reactor. A seven group

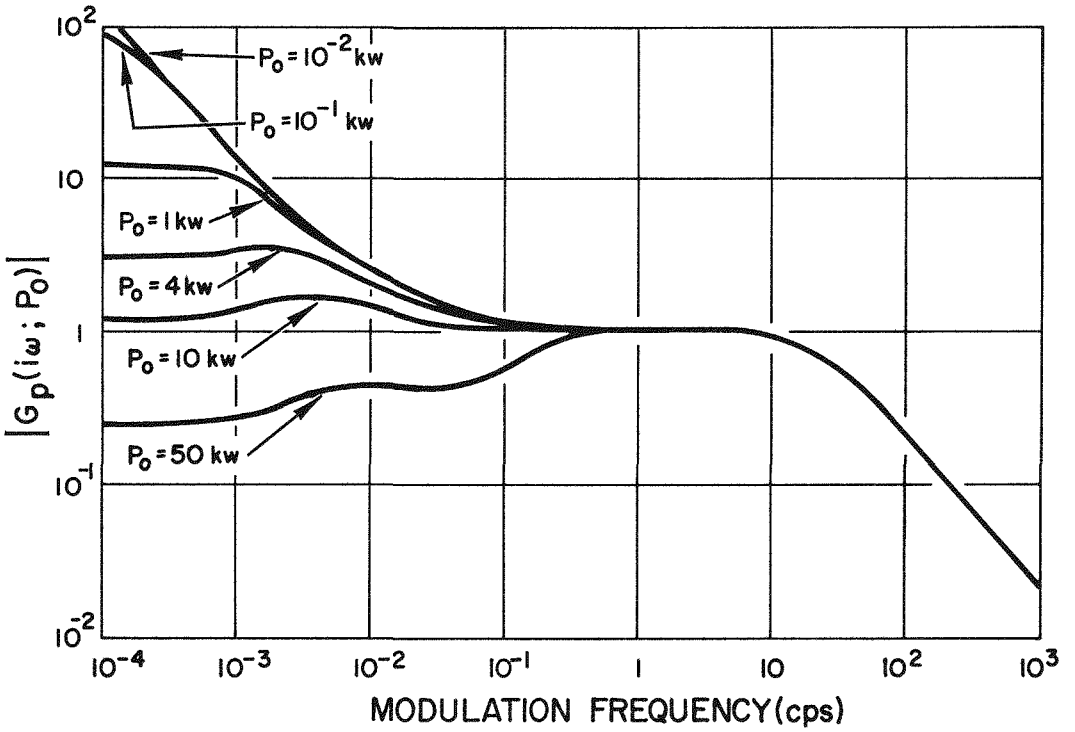

Figure 1. Water Boiler Transfer Function - Amplitude
(six groups of delayed neutrons)

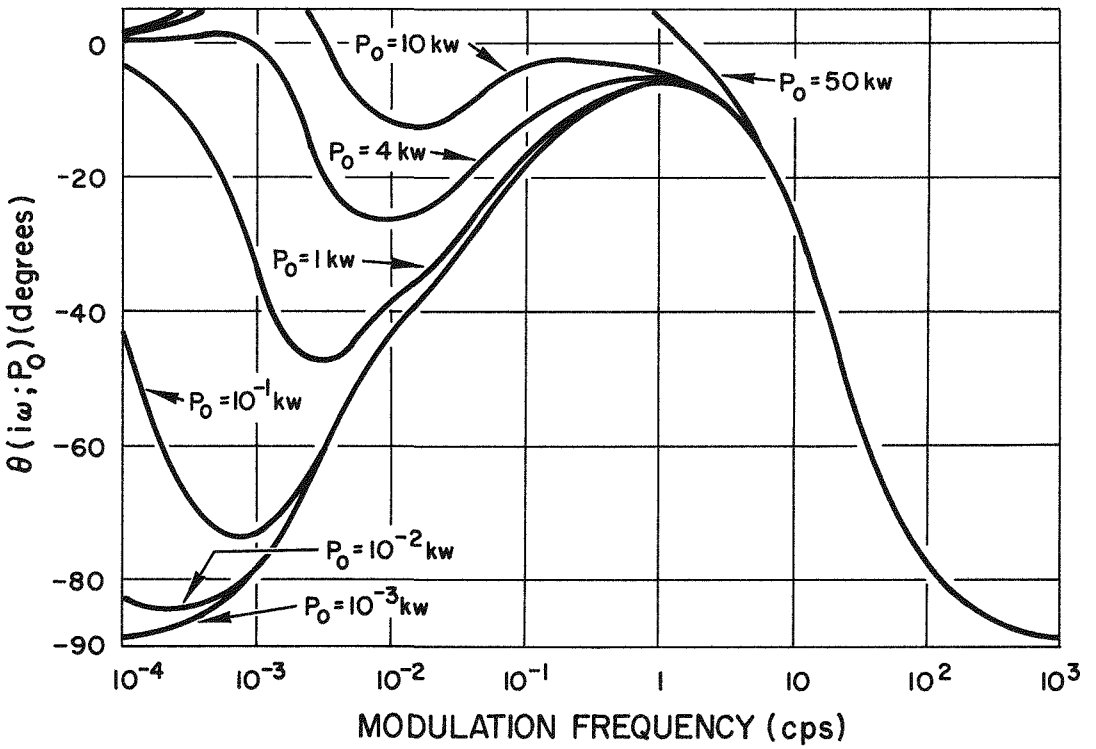

Figure 2. Water Boiler Transfer Function - Phase
(six groups of delayed neutrons)

TABLE I

KINETIC PARAMETERS[2]

Parameter	Value	Units
β	0.008	dimensionless
ℓ	62.5×10^{-6}	sec
K	0.02	°C/kw-sec
G	4.16	cm^3/kw-sec
γ	0.01	sec^{-1}
σ	0.5	sec^{-1}
α^*	-.02	\$/°C
ϕ^*	-.005	$\$/cm^3$

TABLE II

PROPERTIES OF DELAYED NEUTRONS[3]

Group j	Fraction a_j	Decay Constant $\lambda_j (sec^{-1})$
1	0.033	0.012
2	0.219	0.030
3	0.196	0.11
4	0.395	0.30
5	0.115	1.14
6	0.042	3.01

model has been proposed,[4] which describes the neutron lifetime observed in the slower transients as

$$\ell = \ell_0 + \frac{\beta_7}{\lambda_7}, \qquad \ldots (15)$$

where ℓ_0 is the effective lifetime of the neutrons that remain in the core.

At the time of this reactor modulation experiment these seventh group parameters ℓ_0, β_7, λ_7 were not well known. All evidence, however, indicated that the lifetime observed during the slower transients was very closely equal to 62.5 μsec. Thus, one might expect some significant high frequency behavior in the transfer function that may give an insight to the values of these seventh group parameters.

B. DETERMINATION OF ℓ/β

Essentially two methods are available to determine ℓ^* from the experimental reactor transfer function. In the first case the kinetic parameters of the theoretical transfer function are varied to fit with the experimental data. The parameters corresponding the closest to this data would then be considered valid.

The second of these two methods is a result of the high frequency behavior of the theoretical transfer function. Consider Equations 10, 11, and 12 as ω becomes large, and note that

$$A_1(i\omega;P_0) \sim \sum_{j=1}^{m} a_j \qquad \ldots(16)$$

and

$$A_2(i\omega;P_0) \sim \omega \ell^*; \qquad \ldots(17)$$

therefore,

$$\left|G_p(i\omega;P_0)\right| \sim \frac{1}{\omega \ell^*} \qquad \ldots(18)$$

and

$$\angle G_p(i\omega;P_0) \sim \arctan(-\omega\ell^*). \qquad \ldots(19)$$

Thus, the experimental transfer function provides a ready means of determining ℓ/β should one be able to modulate at frequencies greater than the largest of the delayed neutron decay constants.

In the preparation of the experiment and in the final analysis, the emphasis will be placed on phase information. This is done because small changes in the transfer function are manifested more accurately in the phase data.

III. EXPERIMENTAL EQUIPMENT

The performance of this type of experiment to determine the transfer function of a reactor requires a method by which the reactivity may be sinusoidally perturbed over a frequency and amplitude region dictated by theory; a means of determining the instantaneous reactor power; and a technique by which the time delay between any reactivity perturbation and its corresponding power perturbation may be determined.

The following equipment and methods were developed to perform a reactor modulation experiment on the KEWB reactor.

A. MODULATOR

The KEWB reactor oscillator is of the type described by L. G. Barrett as the Mechanical Rotary Modulator.[5] It basically consists of two nested coaxial cylinders inserted in the central exposure tube of the reactor. The nested assembly is equipped with bearings so that the brass outer cylinder, the rotor, is free to rotate about the fixed steel inner cylinder, the stator.

An approximate sinusoidal power modulation occurs as a result of the self-shielding effect created when small rectangular cadmium "shades" mounted on the inner surface of the rotor sweep across sinusoidally shaped cadmium "spots" mounted on the outer surface of the stator. Figures 3 and 4 show the positioning of the spots and shades on their respective cylinders. It should be noted that with this assembly, four perturbation cycles occur for each revolution of the rotor. A typical waveform of the reactivity controlled by this device is shown in Figure 5.

The amount of reactivity is readily changed by the addition or removal of spots. The spots are secured by merely gluing them in place, since the cylinder on which they are mounted does not rotate. Further control of the reactivity can be effected by filling the central bore of the stator with water, thus increasing the worth of the spots.

B. DRIVE MECHANISMS

The first of two separate drive mechanisms consists of a synchronous motor coupled to the rotor through a variable speed transmission and timing belt. With

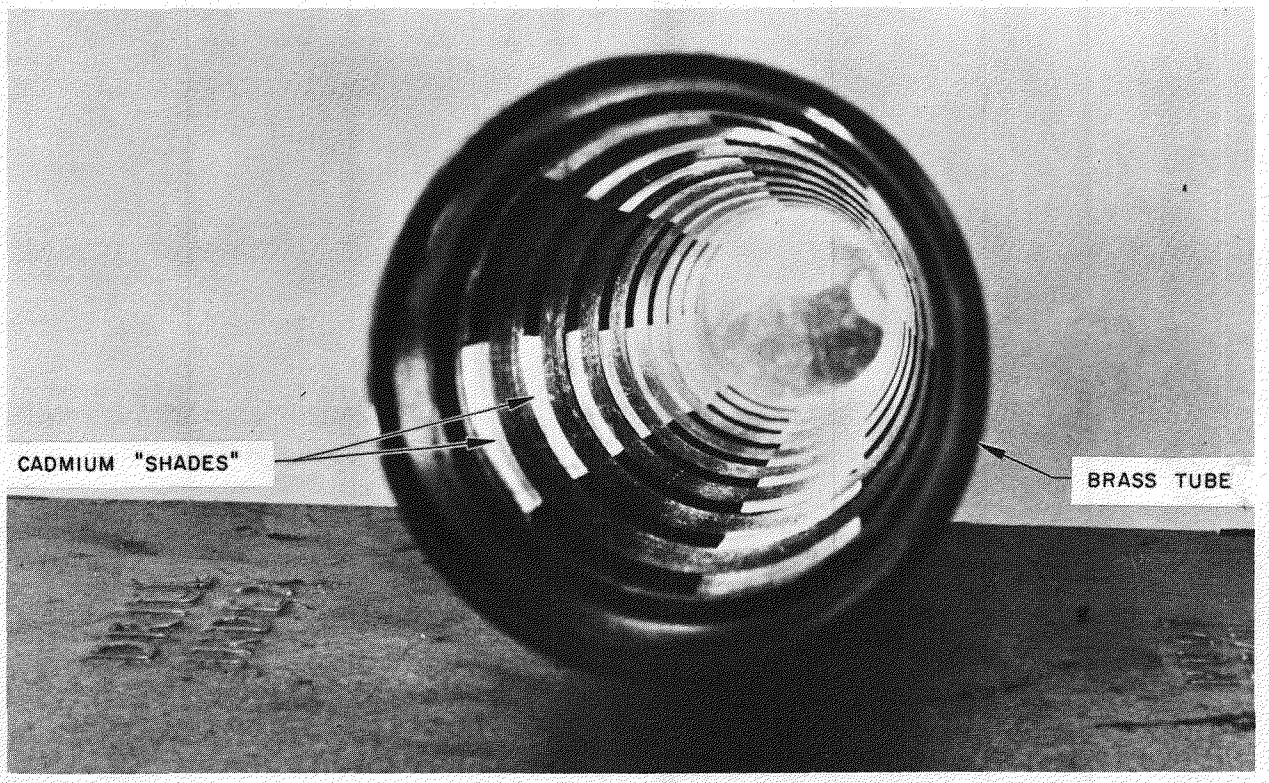

Figure 3. Rotor Shade Assembly

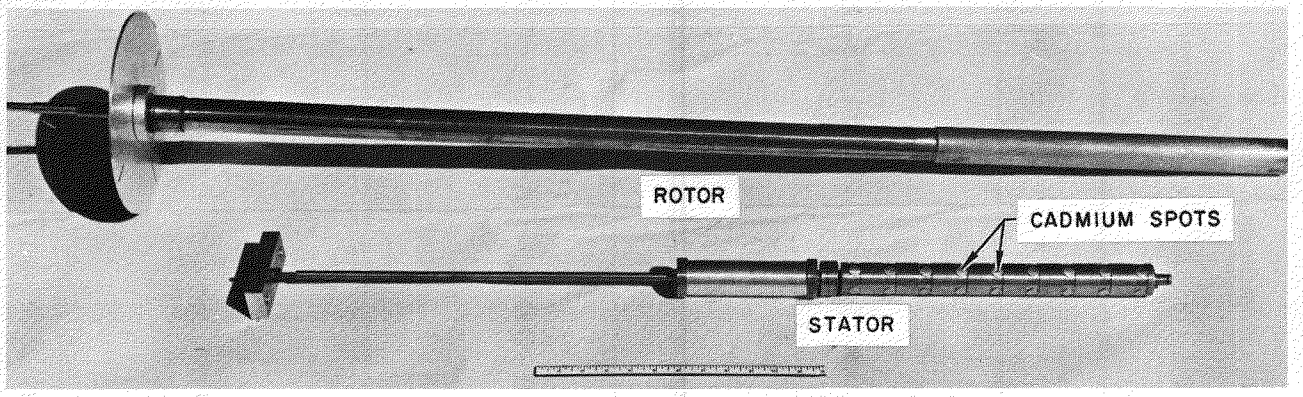

Figure 4. Complete Stator and Rotor Assemblies

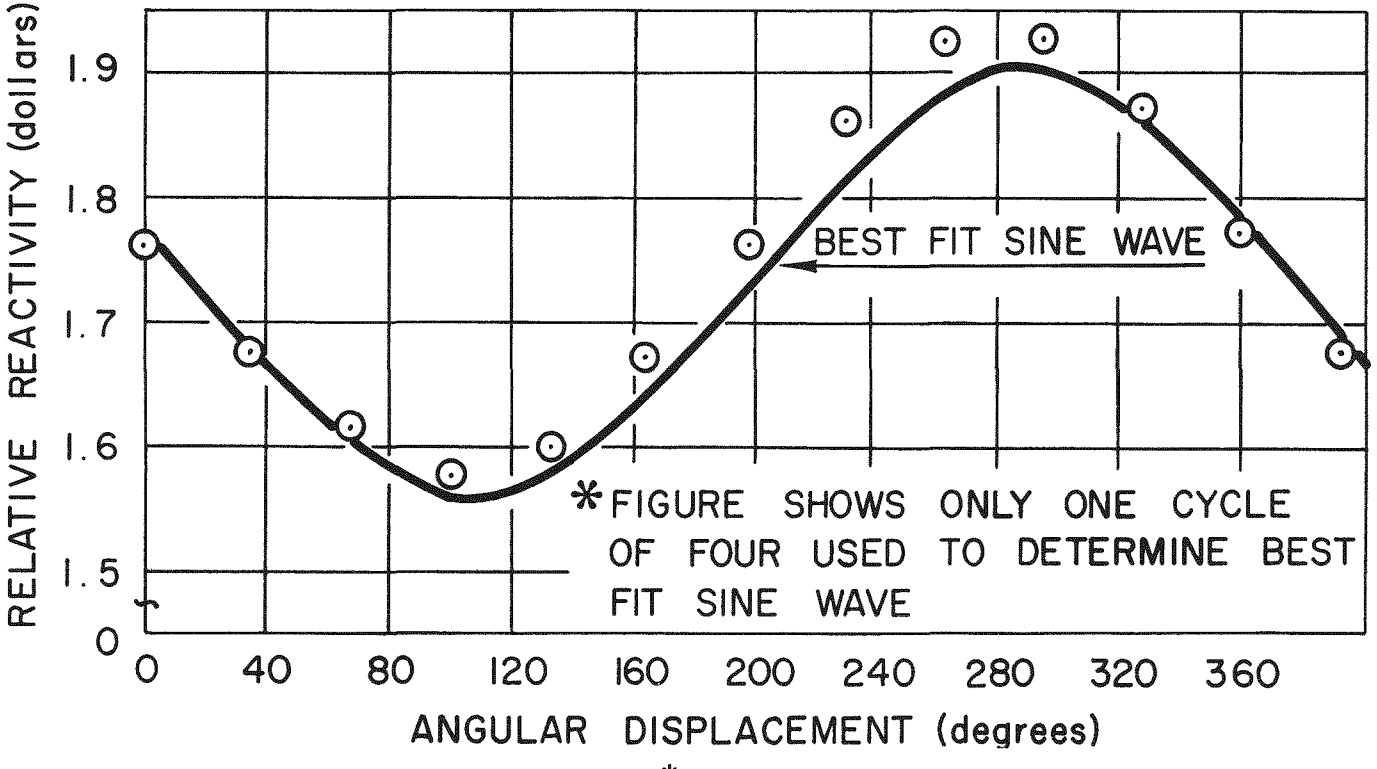

Figure 5. Input Reactivity Waveform* (nine rows of spots and shades plus water filled central bore)

this drive assembly, the speed can be controlled at the reactor console throughout its entire speed range. For the timing pulley configuration used, the frequency range with this device was from 1 to 260 cps.

At perturbation frequencies less than one cps, the variable speed transmission becomes slightly unstable. To overcome this situation, a second drive mechanism is used. In this case, a small synchronous motor is coupled to the rotor by a step gear reducer and timing belt. The pulley configuration here was set to obtain frequencies from 0.022 to 20 cps. The two drive assemblies are shown in Figure 6.

The limits on the complete frequency spectrum are established by practical considerations. The lower limit is the lowest frequency at which the drift of the stable reactor power remains negligible during any complete cycle. At the upper limit, the rotor turns at 3900 rpm. Since the rotating assembly was not dynamically balanced, it was believed that vibration problems might have damaged the central exposure tube at higher angular velocities. The four decades in frequency thus available appeared to be entirely adequate for this study. This, in fact, was later verified by the experimental data.

C. TIMING SIGNAL

One can determine the position of the rotor, and thus the relative position of the spots and shades, by observing an electrical pulse triggered by the rotor. Rigidly attached to the rotor is a circular disk with four slits cut along radii at 90° intervals. A collimated light beam directed at a photoelectric cell is interrupted at all angular positions except where the slits occur. Thus from the photocell circuit, four pips occur for each revolution of the rotor; i.e., one pip for each perturbation cycle. The timing assembly is shown in Figure 6.

If the position of the pip with respect to the reactivity waveform is known, one can compare the pip and the reactor power signal simultaneously and determine the system phase lag. The location of the pip is determined by a static measurement of the reactivity worth of the spot and shade assembly as a function of the angular position of the rotor. The details of this measurement are discussed in Section V.

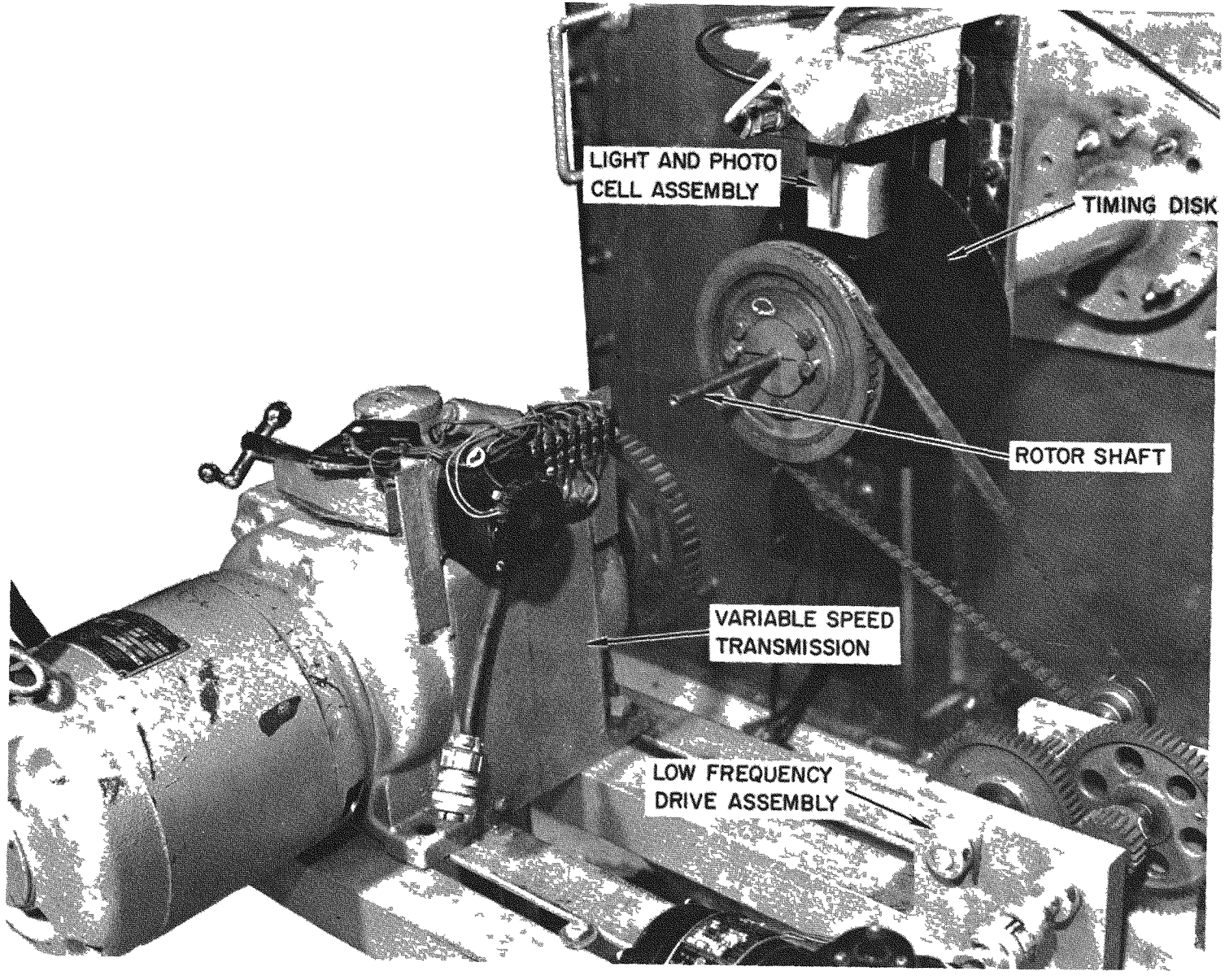

Figure 6. Installed Reactor Modulator Assembly

D. REACTOR POWER DETECTION

The high frequency region over which the experimental transfer function is to be obtained is such that monitoring of reactor power through thermal neutron detection would result in erroneous data. Two important problems occur in this respect.

The first of these is a result of the frequency dependent behavior of the diffusing thermal neutron flux.[6] In this case, both the amplitude and the phase of the measured transfer function would be in error. The second difficulty is the relatively long slowing down time of the thermal neutron detection. As shown in Section VI, this effect is significant at even moderate perturbation frequencies.

To overcome this problem, a boron-10 lined, lead-shielded ionization chamber[7] was wrapped with 1/8-in. cadmium sheeting. As a result, a factor of five was lost in sensitivity, but at the same time this technique greatly reduced diffusion and transit time errors.

Both a cadmium wrapped and an unwrapped chamber were used in the experiment. These were placed in the instrument stringer in the graphite reflector approximately 9 in. from the core surface.

E. AMPLIFICATION AND RECORDING

The basic philosophy of the instrumentation for this experiment design was to keep all instrument errors in a region small enough so that correction factors would not have to be applied to the data. Specifically, to obtain ℓ/β to ± 15% from the phase data, (Equation 19), it is necessary to keep the phase error within ± 4 degrees at the break frequency of the reactor.

The maximum perturbation frequency at which it was planned to operate was something less than 300 cps; thus, an instrument channel with a bandwidth of one kc would introduce a negligible error in amplitude measurements.

The situation is not, however, quite so simple for phase measurements, (the phase error situation is discussed in detail in Section IV). It is important to note, however, that for a single time constant system the required bandwidth for less than 1/2 degree phase lag at 300 cps is 34.4 kc.

The electronic equipment normally used at the KEWB facility for the instrumentation of the transient experiments have the bandwidth characteristics indicated in Table III.

TABLE III

INSTRUMENTATION BANDWIDTHS

Component	Bandwidth
Electrometer Preamp	~ 35 kc
Kintel Amplifier	~ 10 kc
CEC 316 Galvanometer	~ 2 kc
Tektronic Dual Beam Oscilloscope Model 502	~ 100 kc

With the requirement that this equipment be used and that the phase error be kept to a minimum, the system block diagram shown in Figure 7 was devised. All of the components indicated in Figure 7 are conventional reactor instrumentation components except perhaps the suppressor. The suppressor provides a means of biasing to zero the signal from the chamber due to the equilibrium reactor power. It is essentially a variable voltage supply connected to the end of the preamp input resistor that would normally be grounded.

Provided as an integral part of the suppressor is a switch which, when closed, will raise the voltage at the grid of the electrometer tube by 1% of the dc component previously biased to zero. As a result, a signal proportional to the equilibrium reactor power can be recorded by merely momentarily closing the switch.

The calibrated audio oscillator and the single beam oscilloscope are used to determine the perturbation frequency. The signal from the audio oscillator is beat with the photocell timing pip and a modified Lissajous pattern is obtained on the oscilloscope. When the pattern is stable, the modulation frequency is that of the audio oscillator, or of some harmonic thereof.

With the instrument configuration shown in Figure 7, the phase lag of the reactor power can be determined from the oscilloscope photographs without correcting the large error introduced by the low bandwidths of the amplifier and galvanometer. At the same time, however, the galvanometer can record many perturbation cycles from which the percent modulation can be accurately obtained.

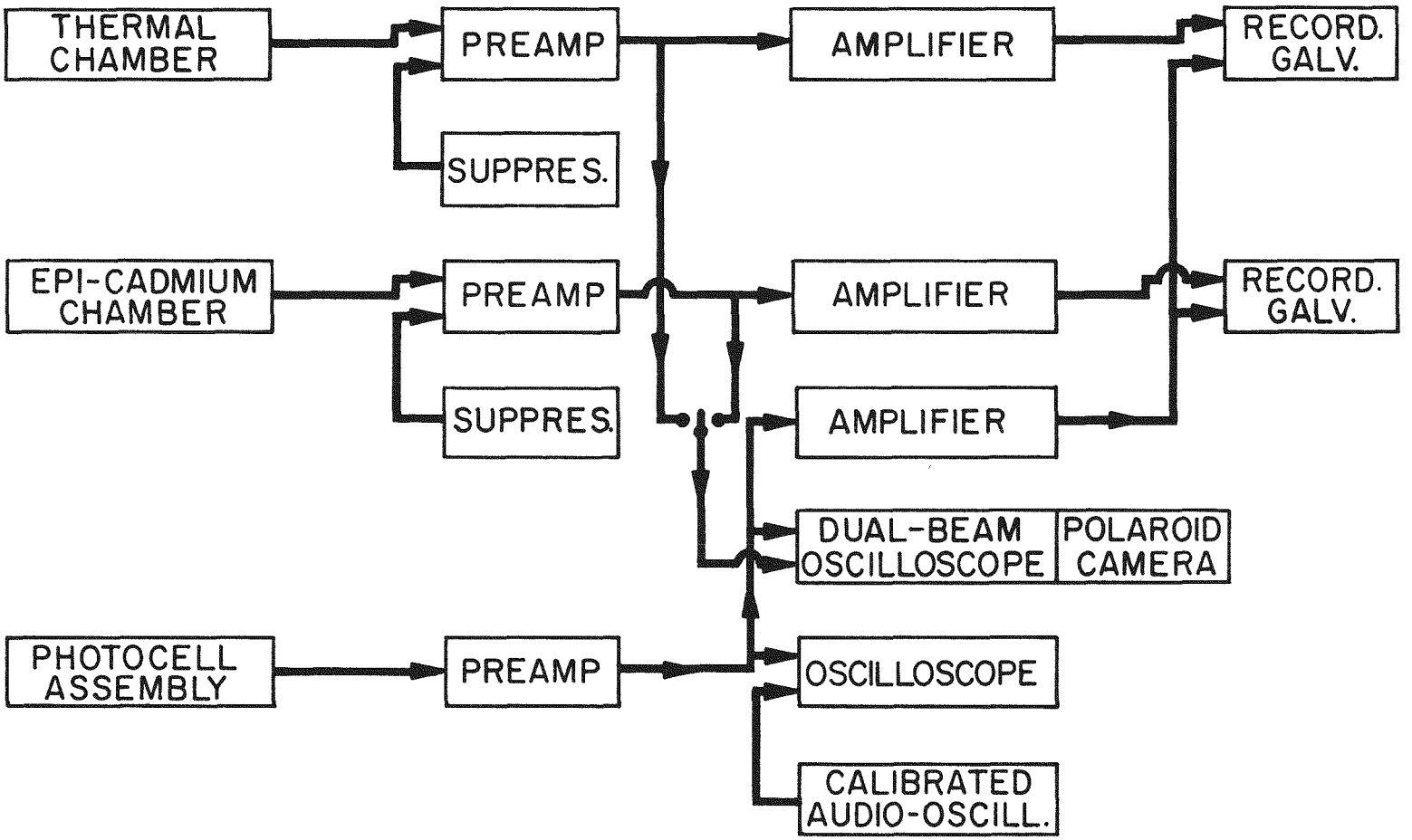

Figure 7. Amplification and Recording System - Block Diagram

IV. MEASUREMENT ERRORS

As indicated in the previous section, the main problem in the instrumentation of an experiment of this type is the introduction of extraneous phase lags. The most significant of these phase lags are listed and briefly discussed.

A. NONLINEAR REACTOR MODULATION

To utilize the reactor oscillator technique in an experimental determination of ℓ^*, the conditions of the transfer function derivation must be met. Specifically, the reactor must be operated in the linear region, i.e., the percent modulation of the reactor power must be small; thus, the large signal to noise ratio desired for good measurements is limited by the nonlinear effects.

A knowledge of the region in which these nonlinear effects become significant can be obtained from Z. Akcasu's general solution to the reactor kinetics equations without feedback.[8] These methods can be applied to the water boiler as a result of the negligible temperature and void feedback effects at the perturbation frequencies of interest.

The frequency range that appears to produce the most useful information concerning ℓ^* and the correct group model, is in the region where the effects of six group delayed neutrons are negligible, i.e., where Equations 16 through 19 apply. If, in fact, one considers such a region in a sinusoidally perturbed reactor, the neutron flux can be written as a series of harmonics; specifically,

if

$$\rho_1(t) = \rho_0 \sin(\omega t),$$

then

$$P(t) = P_0 \left[1 + \rho_0^* \left| Z_1 \right| \sin(\omega t + \theta_1) \right.$$

$$\left. - \frac{1}{2} \left(\rho_0^* \right)^2 \left| Z_1 Z_2 \right| \cos(2\omega t + \theta_{1,2}) + \ldots \right] . \qquad \ldots (20)$$

It was previously mentioned that in a determination of ℓ^* Equation 19 would be most useful. With this in mind, the main interest is in the error introduced by the higher order harmonics in the phase measurements. For excess reactivities much less than a dollar, the error introduced by the second harmonic need only be considered.

A pure sine wave passes through its mean value at multiples of 180°; thus, if one determines the value of ωt at which the distorted waveform passes through its mean value, he will have a measure of the phase error due to nonlinearities. Specifically, if P(t) in Equation 20 is set equal to P_0, then

$$\sin(\omega t) = \frac{\rho_0^*}{2} \left|Z_2\right| \cos(2\omega t + \theta_2). \qquad \ldots(21)$$

Calculations of this form prove to be invaluable in preparing an experiment of this type and in analyzing the resulting data for nonlinearities. Should one have an approximate transfer function available prior to the performance of the experiment, he can determine reasonably accurate values of the maximum permissible percent modulation as a function of allowable phase error, frequency, excess reactivity, and stable reactor power.

The nonlinear error of the results can be calculated from the measured transfer function and excess reactivity. Figure 8 presents the nonlinear phase error for the data of this experiment (as calculated from Equation 21) for the maximum reactivity loading of the oscillator.

B. NEUTRON DIFFUSION

The use of epi-cadmium neutrons in determining reactor power greatly reduces amplitude and phase errors due to diffusion effects. An indication of the remaining phase error can be determined from a knowledge of the slowing down time of an epi-cadmium neutron.

The slowing down time of a neutron from energy E_1 to E_2 is given by Glasstone[9] as

$$t = \frac{\sqrt{2m_0}}{\xi \bar{\Sigma}_s}\left(\frac{1}{\sqrt{E_2}} - \frac{1}{\sqrt{E_1}}\right), \qquad \ldots(22)$$

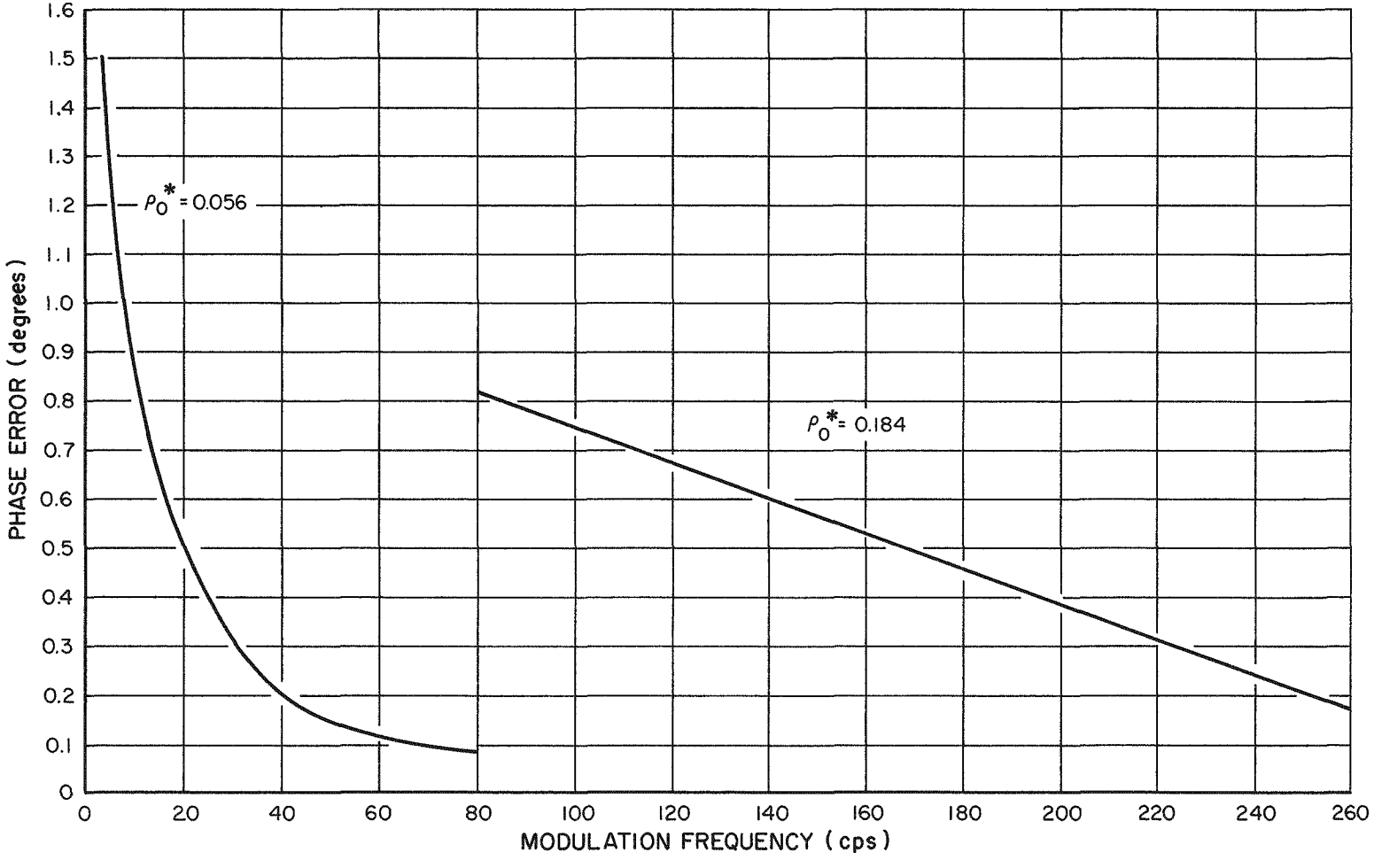

Figure 8. Nonlinear Phase Error of Data

where, for graphite

$$\xi = 0.158$$

$$\overline{\Sigma}_s = 0.30 \text{ cm}^{-1}.$$

Thus, the time required in slowing down from fission energy ($\sim$2mev) to the cadmium cut-off ($\sim$0.3 ev) is 4.65×10^{-5} sec. The phase shift accounted for by this effect is presented in Figure 9. It is important to note, however, that the errors indicated in Figure 9 are correct, provided all neutrons are at 0.3 ev. The actual experimental error must, therefore, be less than indicated here.

C. INTERNAL ION CHAMBER EFFECTS

There are essentially two effects that become important when an ionization chamber is used in a phase measurement. In the first case, the interelectrode potential must be sufficient so that space charge distortion and resulting ionic recombination is small. Secondly, this potential must be such that the ion transit times are small.

Huntsinger has determined the interelectrode potential as a function of ion current and the maximum permissible phase error for the chambers used in these measurements.[10] His results, as applied to this experiment, are summarized in Figure 10.

D. CHAMBER TIME CONSTANT

The chamber and lead capacitances, combined with the variable input resistor at the grid of the electrometer tube, produce a single time constant system. As such, the phase lag introduced here can be written as

$$\theta_{RC} = \arctan(\omega RC) \qquad \ldots(23)$$

The experimental error, as computed from Equation 23 is presented in Figure 11.

E. PREAMP AND OSCILLOSCOPE BANDWIDTHS

The break frequencies of both the preamp and dual beam oscilloscope are such that their combined error will be less than 1/2 degree for all perturbation frequencies.

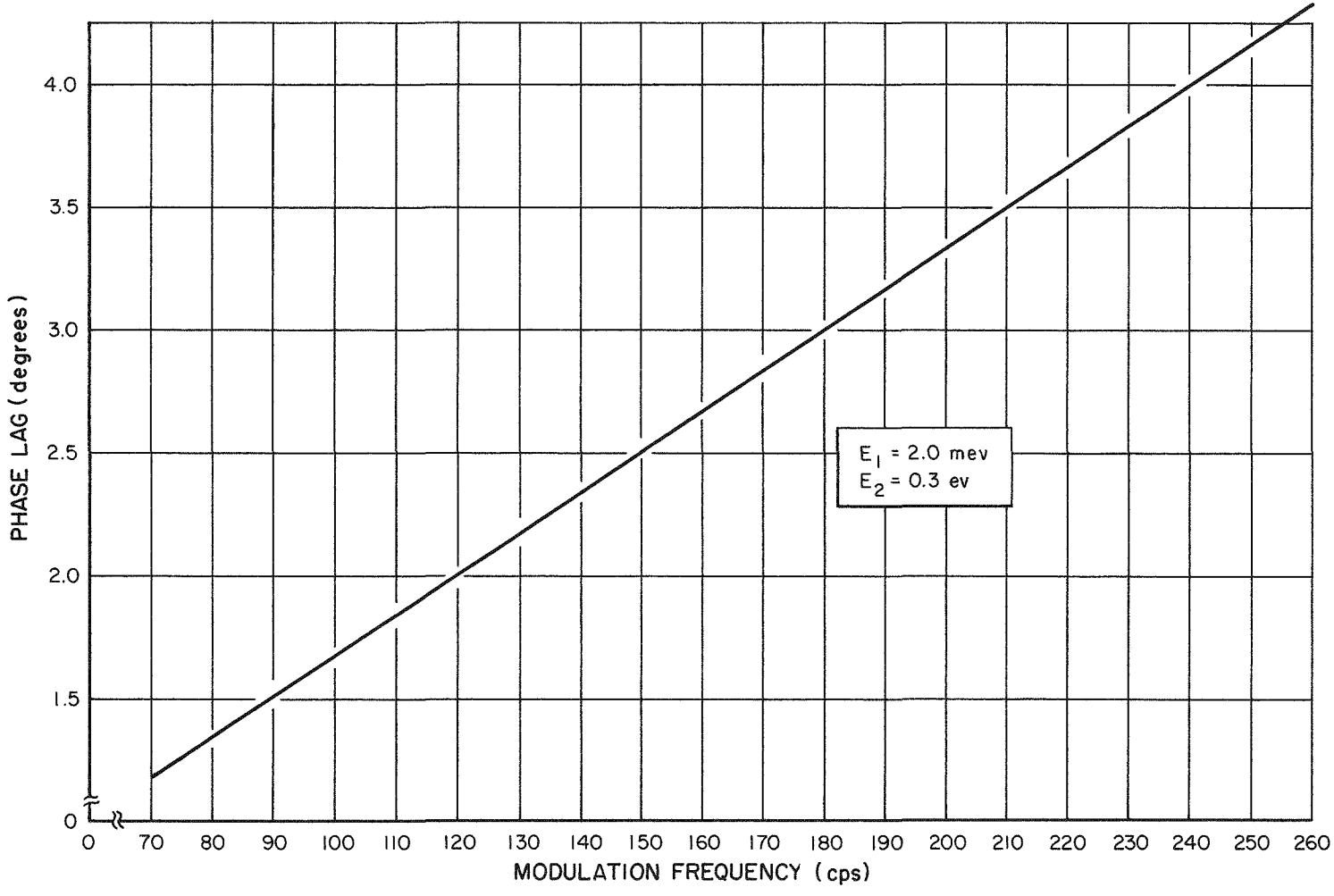

Figure 9. Phase Error Due to Slowing Down Time

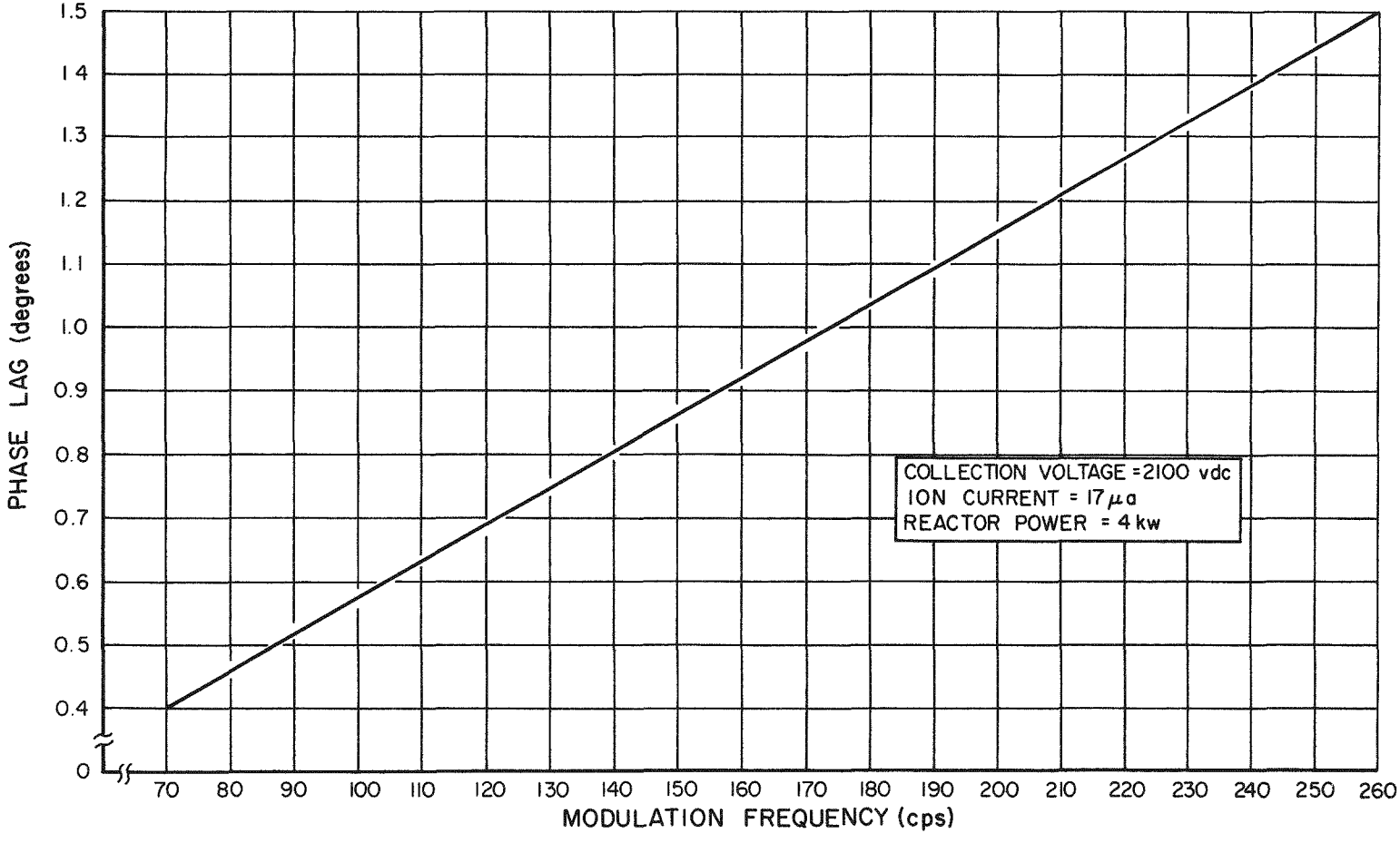

Figure 10. Phase Error Due to Internal Ion Chamber Effects

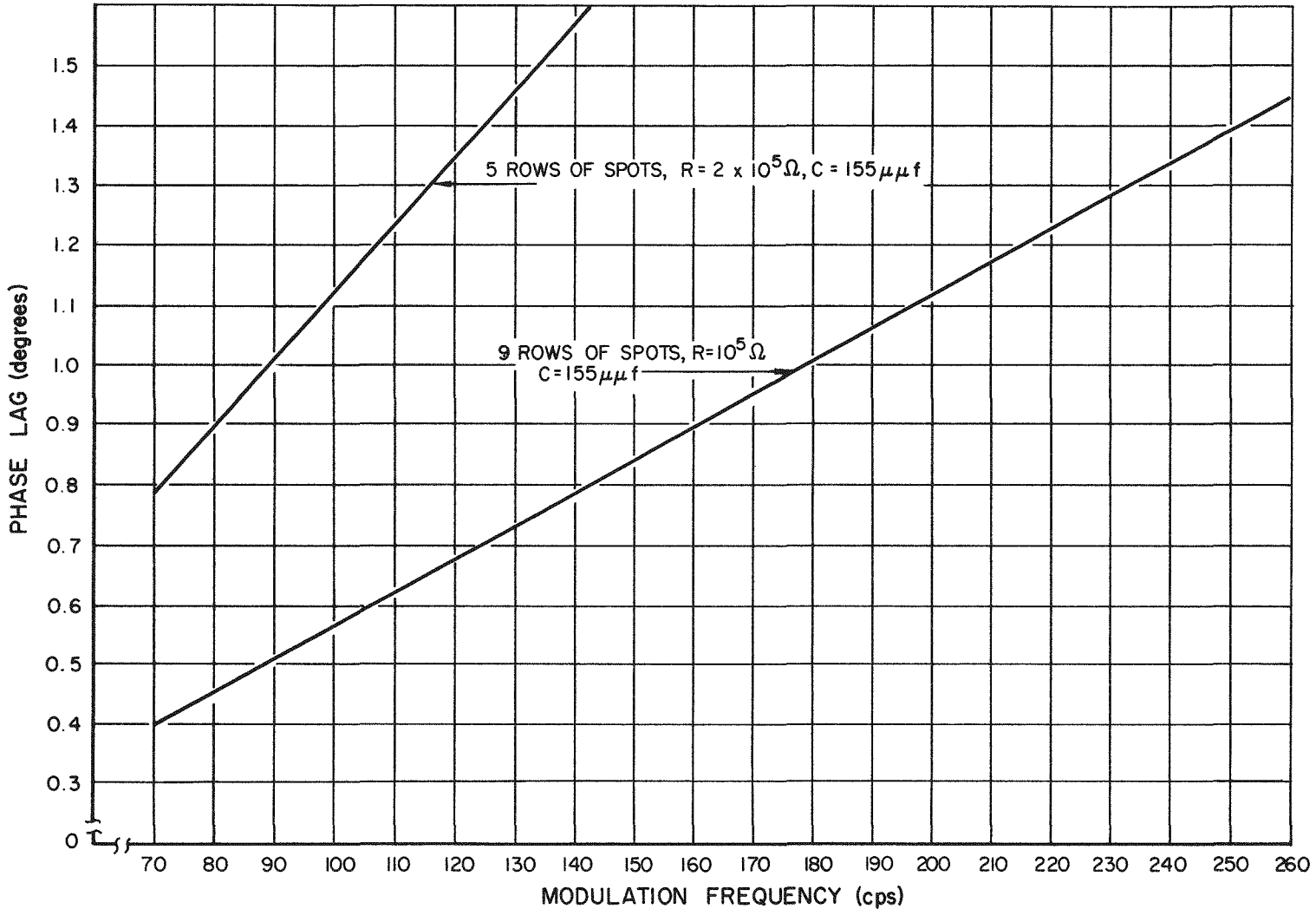

Figure 11. Phase Error Due to Input Capacitance

F. TOTAL MEASUREMENT ERROR

The calculated total phase measurement error of this experiment is presented in Figure 12. It is believed that this plot shows a maximum experimental error since more than half of its amplitude is made up of the error due to neutron slowing down time as determined from Equation 22.

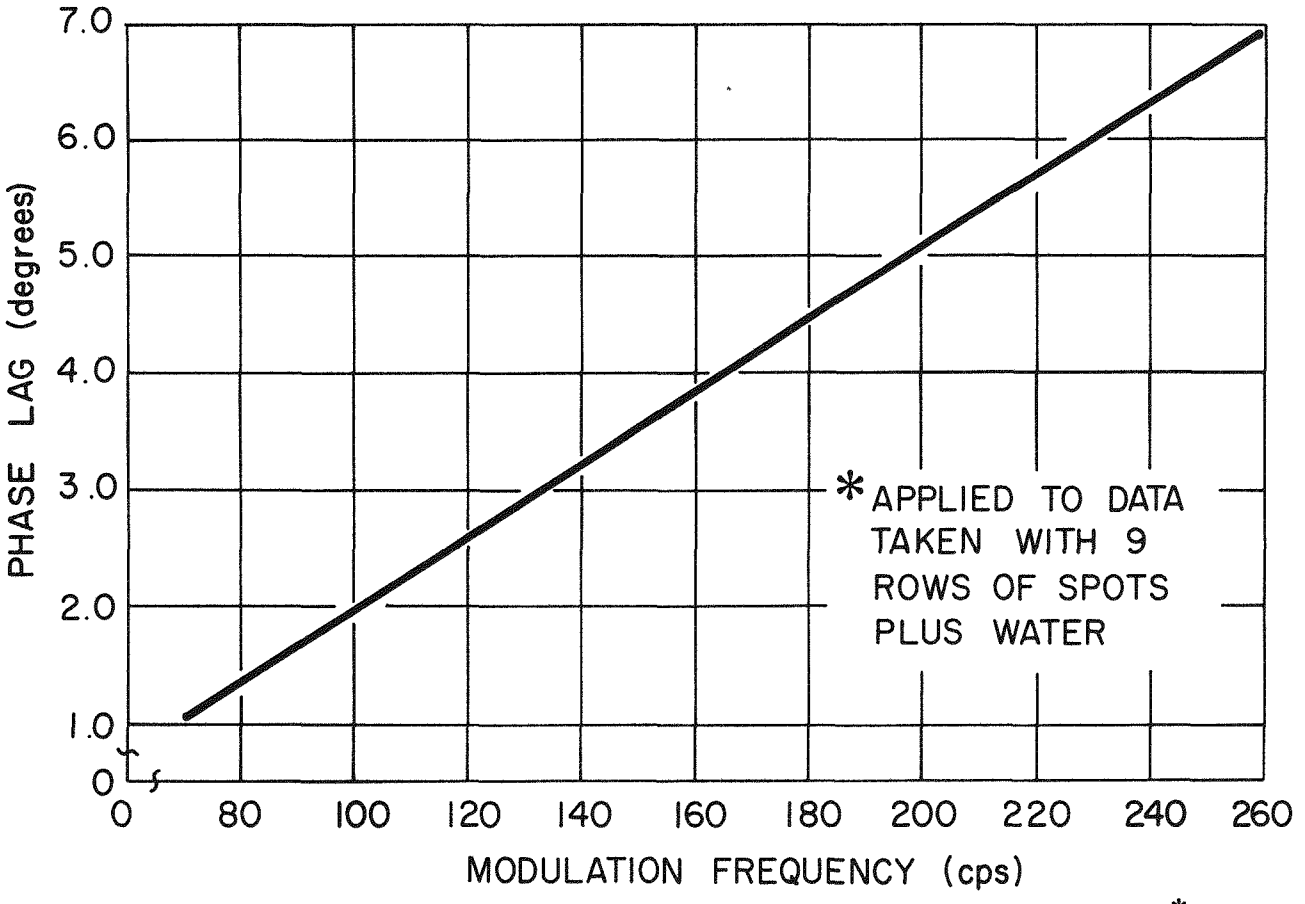

Figure 12. Calculated Maximum Total Phase Measurement Error*

V. EXPERIMENTAL PROCEDURES

A. PREPARATION

An outline for the performance of the experiment can be obtained with a knowledge of the analytic transfer function, the approximate magnitude of the input reactivity, and with a consideration of some practical limitations.

Those practical limitations which one has little control over are listed in Table IV. The chamber sensitivities are measured with the chambers as close as possible to the core surface, and the capacitance value is measured with an absolute minimum lead length. The inter-electrode potential is the maximum usable value without breakdown within the chamber. The modulation voltage indicates the minimum modulation signal from the power channel required for a reasonable signal-to-noise ratio.

TABLE IV

PRACTICAL LIMITATIONS

Limitation	Value
Ion Chamber Sensitivity	
Cadmium wrapped chamber	4.3 μa/kw
Unwrapped chamber	21.0 μa/kw
Ion Chamber and Lead Capacitance	120 $\mu\mu$f
Interelectrode Potential	2100 vdc
Modulation Voltage	0.1 vac (peak-to-peak)

With these four items in mind, one can determine as a function of perturbation frequency and permissible phase error, the limits of operation of the following parameters:

1) Maximum preamp input resistance (Equation 23);

2) Maximum reactor power (Figure 10);

3) Minimum reactor power (Equations 20 and 23).

The first two of these are straightforward determinations; the third is determined by first finding the current necessary to produce a 0.1 volt modulation signal across the maximum input resistance (Equation 23). A knowledge of the maximum percent modulation, a result of the nonlinear analysis, will then permit one to fix the minimum reactor power.

However, for close error tolerances, the minimum power requirement by time constant considerations is actually greater than the maximum power limitation imposed by ion mobility restrictions. As a result, it is necessary to expand the allowable error range at the higher perturbation frequencies. With due consideration of these practical limitations, the approximate values of input reactivity, preamp resistors and reactor power can be predetermined, thus greatly facilitating the experimental procedures.

B. PERFORMANCE

First on the agenda of experiments was to determine the location of the timing pip with respect to the input reactivity waveform. This was accomplished by bringing the reactor to critical at some arbitrary stable power with the modulator completely installed, but not rotating. The position of the control rods and thus the relative reactivity was noted. The modulator was then rotated for four seconds at its lowest frequency, 0.022 cps, and the new critical rod position was determined and recorded. During the four seconds of rotation the pip signal was fed to an oscilloscope and the occurrence of the pip was noted as so many seconds of angular rotation after the preceding critical rod position. This procedure was repeated until several complete reactivity cycles had been obtained.

In this manner, a plot of the angular rotation time versus reactivity clearly indicates the position of the pip and its relation to the reactivity waveform. A typical waveform thus obtained and a true best fit sine wave are shown in Figure 5.

The majority of the modulation experiments were made at a stable power of four kw. This level was that indicated by pre-experiment analysis as essentially optimum with regard to the error situations discussed in Section IV.

Some modulation was done at a stable power of ten watts with somewhat unsuccessful results. Measurements were made only with one row of spots and shades, and as a result the signal became noisy at frequencies above one cps. In addition, the few measurements that were taken at ten watts required an

extremely high preamp resistance, thus introducing a very large phase error at almost all perturbation frequencies.

A summary of the regions over which the data were taken and the conditions of the measurements are presented in Table V. At each measurement point photographs were taken; five of the signal from the cadmium wrapped chamber, two of the signal from the unwrapped chamber, and an oscillograph trace of both channels.

One problem arose when the change from five to three rows of spots was made. At that time it was noticed that the stator was not rigidly attached to the reactor structure, resulting in the possibility that a small angular rotation of the stator had occurred. This rotation would change the position of the timing pip with respect to the reactivity waveform, and if uncorrected, would result in an error in the phase measurements.

This situation was corrected and the procedure for determining the location of the timing pip with respect to the reactivity waveform created by three rows of spots was repeated.

TABLE V

DATA SUMMARY

Absorbers	Measured Reactivity (ρ_0*)	Reactor Power (kw)	Cd-wrapped R_{preamp} (ohms)	Unwrapped R_{preamp} (ohms)	Frequency Range (cps)
9 rows + H_2O	0.184	4	10^5	10^5	50 to 260 in 10 cps intervals
5 rows	not measured	4	2×10^5	2×10^5	50 to 100 in 10 cps intervals
3 rows	0.056	4	5×10^5	2×10^5	5, 10, 14, 20, 24 etc. to 70
1 row	not measured	4	5×10^5	2×10^5	1, 2, 6, 10, 14, 20
1 row	not measured	4	5×10^5	2×10^5	0.218
1 row	not measured	4	5×10^5	2×10^5	0.022
1 row	not measured	0.010	10^8	10^8	0.022, 0.0218, 1, 2, 6, 10, 14, 20

VI. DATA TREATMENT AND RESULTS

A. REPRESENTATIVE DATA

Typical oscillograph traces showing the timing pips and the step proportional to stable power are shown in Figures 13 and 14. Figures 15 and 16 show representative photographs of the epi-cadmium signal and the timing pip.

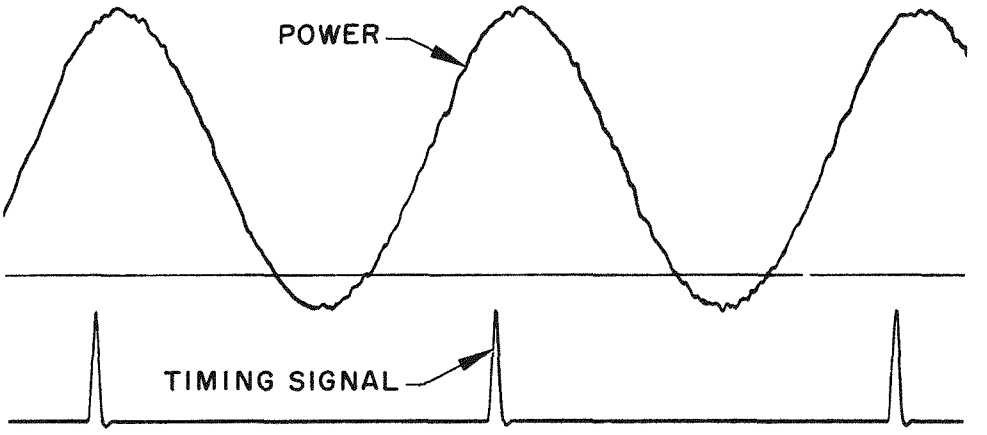

Figure 13. Representative Oscillograph Data
(indicating timing signal)

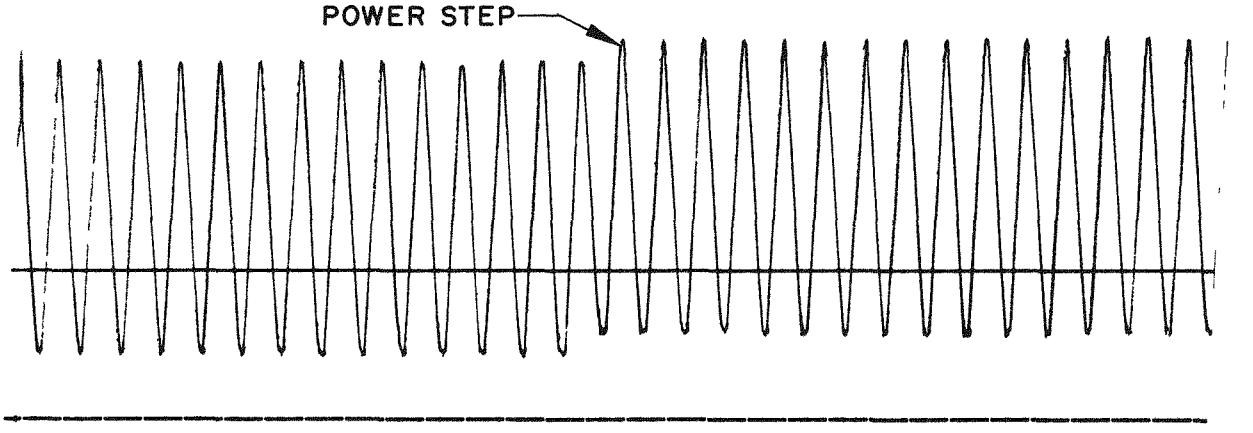

Figure 14. Representative Oscillograph Data
(indicating power step)

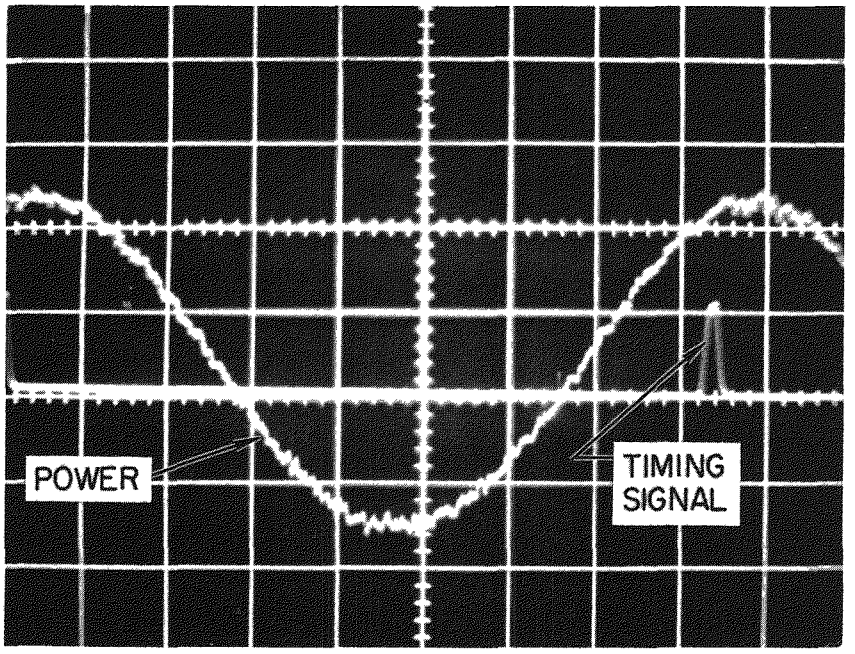

Figure 15. Representative Oscilloscope Data
(low frequency, 30 cps)

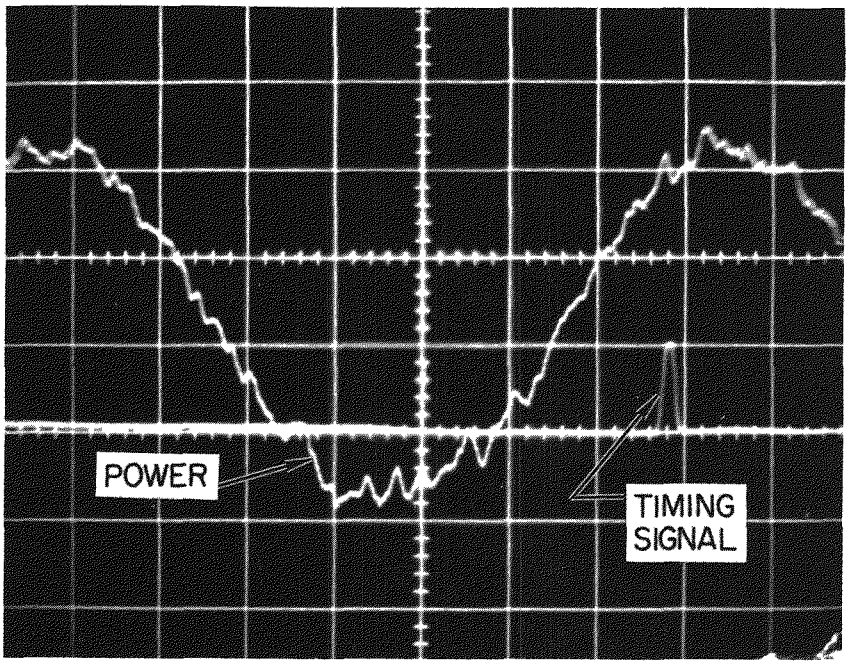

Figure 16. Representative Oscilloscope Data
(high frequency, 260 cps)

B. DATA REDUCTION TECHNIQUES

The percent peak-to-peak modulation is obtained directly from the ratio of the peak-to-peak value of the modulated power to the height of the stable power step. This is valid since the step represents exactly one percent of the stable power. These measurements were made to an accuracy of 0.010 in.

The determination of the phase lags were made by digitalizing the photographs and treating the results by a sine wave fitting program on the IBM-709. The digitalizing was accomplished by reading the amplitude of the waveform at intervals of one mm starting at the midpoint of the timing pip's leading edge. These measurements were made to an accuracy of 0.005 in. No smoothing was done in the digitalizing process.

The IBM-709 program input required, in addition to the power data, an accurately known perturbation frequency (distance between pips) and in turn computed the amplitude and phase of the fundamental harmonic of the modulated power. The phase was computed with respect to the timing pip, thus necessitating the addition of a phase correction factor to obtain the phase with respect to the input reactivity. This correction factor was obtained from the measured relationship of the pip with respect to the reactivity waveform.

The only remaining factors necessary to determine the experimental transfer function were the magnitudes of the input reactivities. Two of the input waveforms, nine rows of spots plus water, and three rows and no water, were subjected to the above mentioned curve fitting program and their amplitudes were recorded as 0.184 and 0.056 dollars respectively.

C. STATISTICAL ANALYSIS

The data for the thermal neutron phase lag were not treated statistically since only one or two measurements were made at each frequency.

All of the remaining data were treated by the Student's "t" test for 95% confidence limits.

D. PRESENTATION

The amplitude of the normalized KEWB transfer function obtained at a four kw stable power is presented in Figure 17. This is a plot of the data normalized to the computer determined reactivities for three and nine row cases. The reactivities for the one and five row sections are extrapolations.

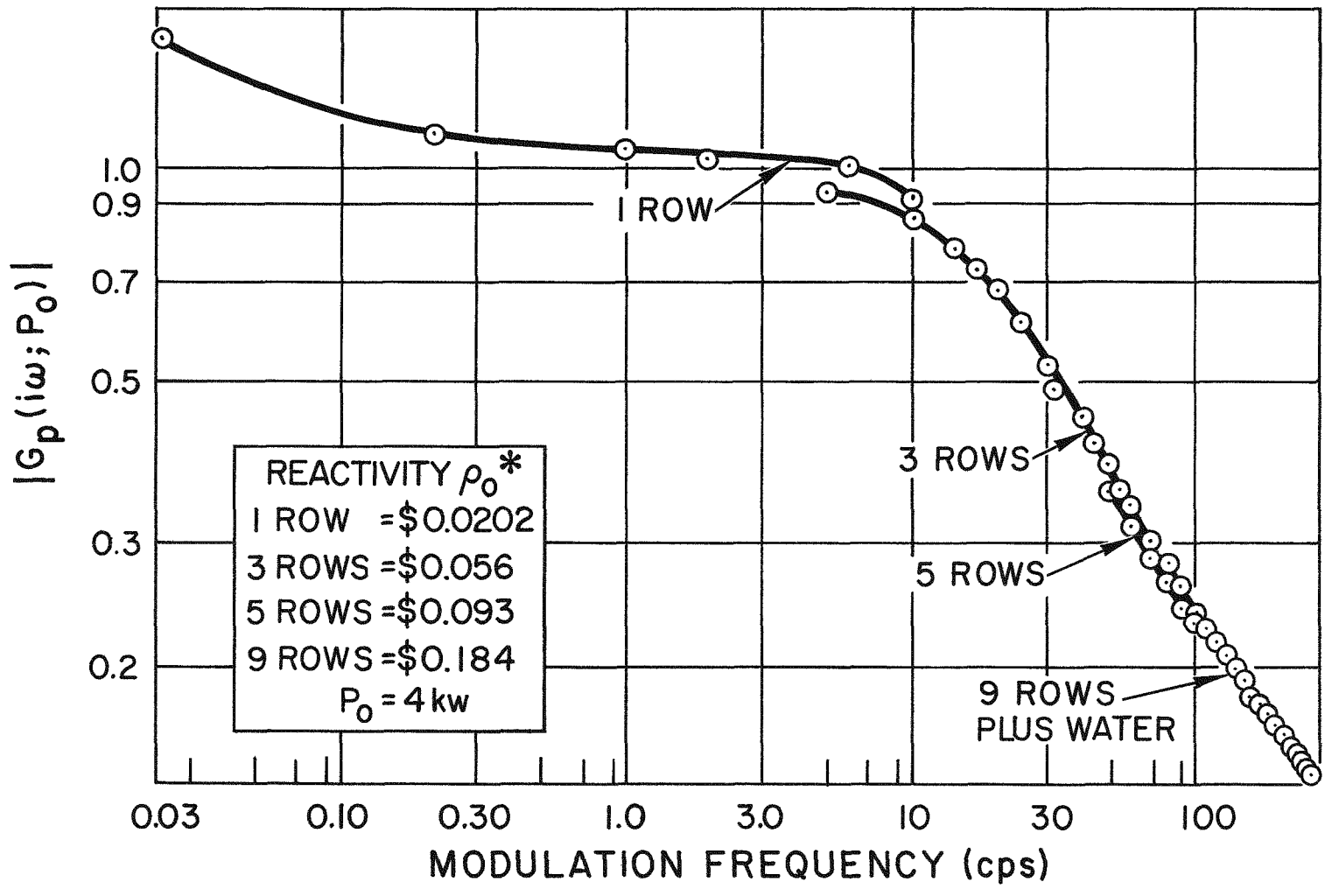

Figure 17. Measured Reactor Transfer Function - Amplitude (unsmoothed)

The discontinuities between the data points are due to errors in the assumed values of the reactivities. This plot may be smoothed since only the shape, and not the absolute magnitude is of prime importance in this study. The smoothed plot along with the required reactivity values is presented in Figure 18.

The four kw phase data, as recorded, are presented in Figure 19. The data exhibit a considerable amount of scatter, and in two cases, show step discontinuities. There appear to be only two rational explanations for these steps. The relationship between the stator and the rotor could change and introduce such an error. In fact, as previously mentioned, slippage was noted during the change from five rows of spots to three rows. It is entirely possible that the position of the stator changed during the spot removal process of nine rows to five rows. It does not, however, appear quite as likely that slippage occurred during the three to one row change, since it was believed at the time that the slippage problem had been corrected.

The other factor that could have caused the discontinuities is the difference in reactivity waveforms for each case used. Timing pips were located only for the nine and three row cases; thus any difference in the waveforms between the nine and five row cases and the three and one row cases would be reflected directly as a constant phase error. In this respect, it is interesting to note that both steps are of the order of 10 degrees, and as such, could easily be accounted for by this effect.

In either case, it is believed that the absolute values of the three and nine row cases are accurate. The four kw phase transfer function normalized to the three and nine row data is presented in Figure 20.

Figures 21 and 22 present the experimental transfer function as compared to various analytic models of the reactor. The six group model is identical to that presented in Section II. Model 1 is that seven group model which appears to fit the data most accurately. Model 2 is that predicted by theoretical considerations.[11]

In the interest of determining the direct cause of discrepancies between theoretical and experimental plots a calculation of the independent effect of ℓ_0, β_7, and λ_7 was made. If these parameters had significant individual effects on the transfer function one would perhaps be able to determine the value of a

particular parameter to an acceptable accuracy. Figures 23 through 28 show the effects of the individual parameter changes on the amplitude and phase of the transfer function.

An interesting sidelight to the objectives of this experiment is presented in Figures 29 and 30. The transfer functions presented here were obtained under identical amplification and recording conditions; the only difference existed in the cadmium wrapping of the chamber from which the epi-cadmium power signal was taken.

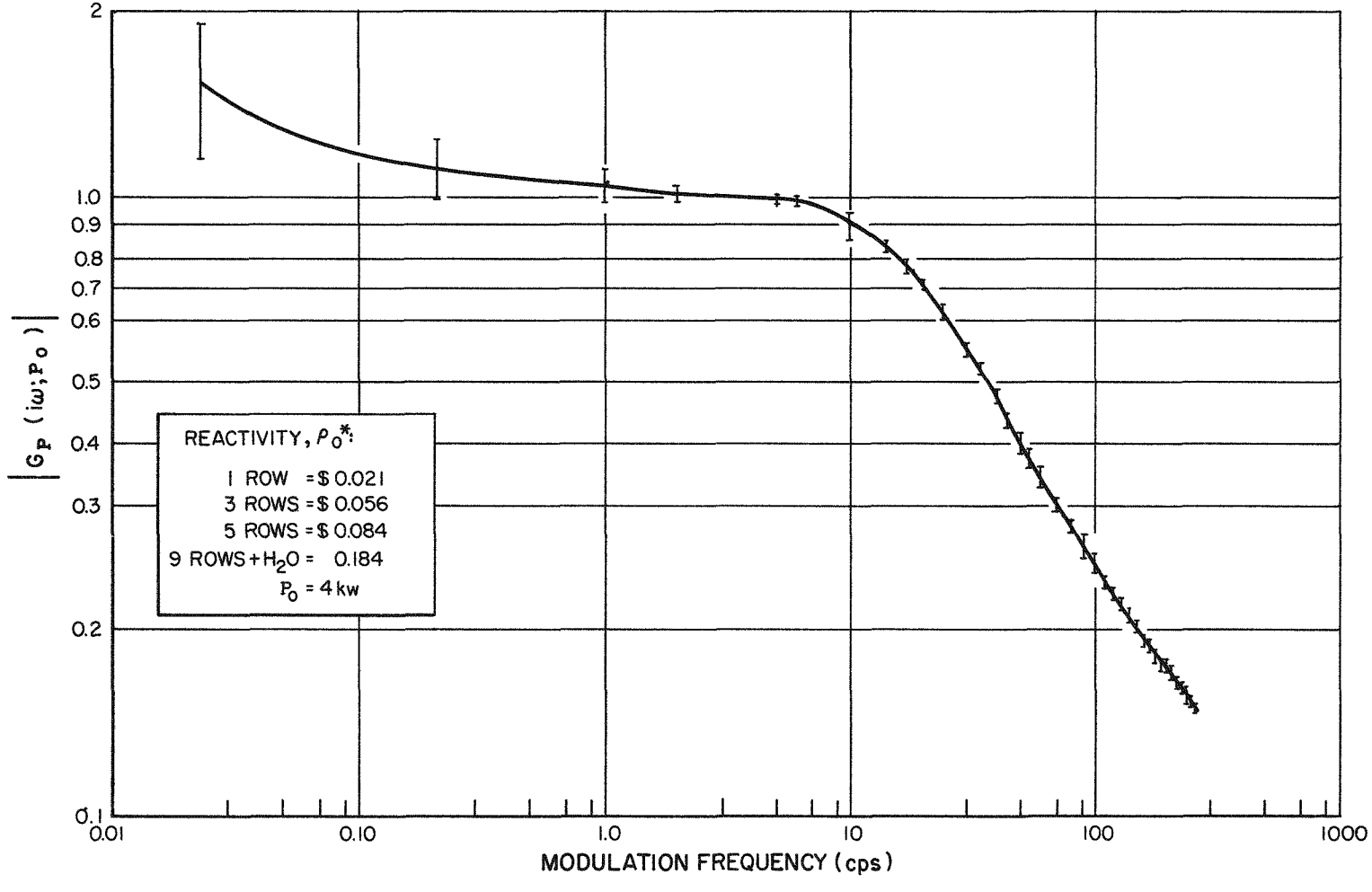

Figure 18. Measured Reactor Transfer Function - Amplitude (smoothed)

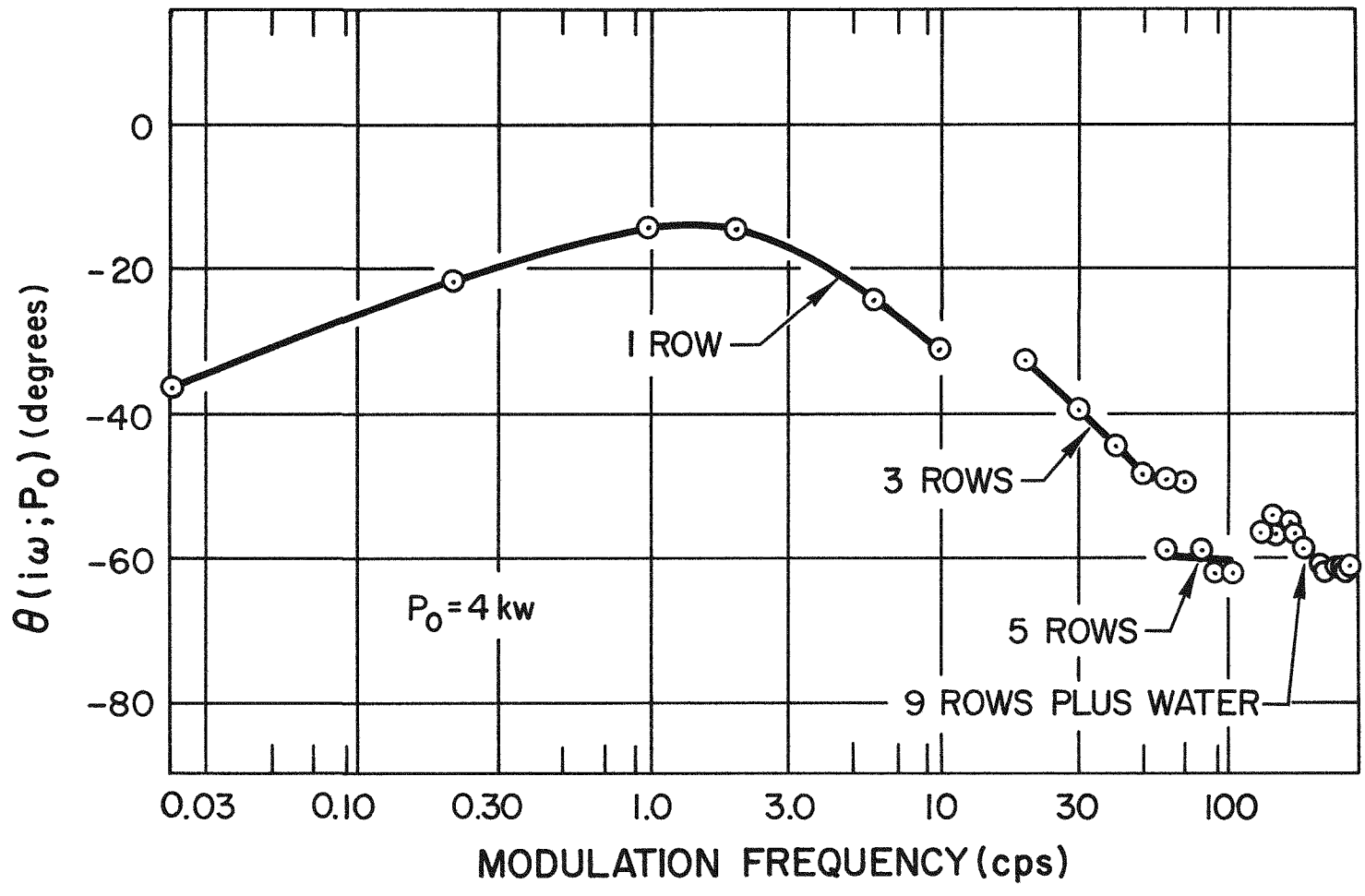

Figure 19. Measured Reactor Transfer Function - Phase (unsmoothed)

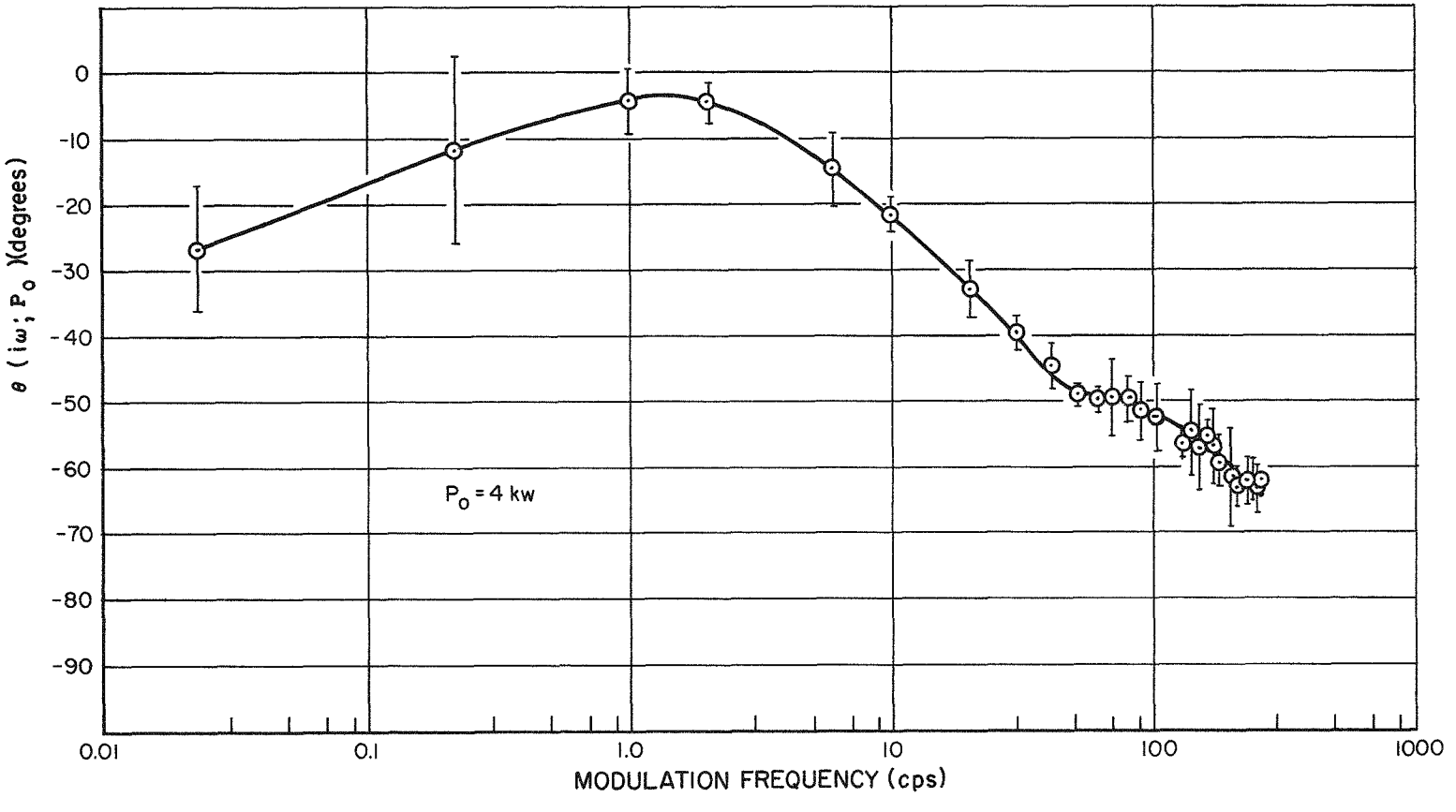

Figure 20. Measured Reactor Transfer Function - Phase (smoothed)

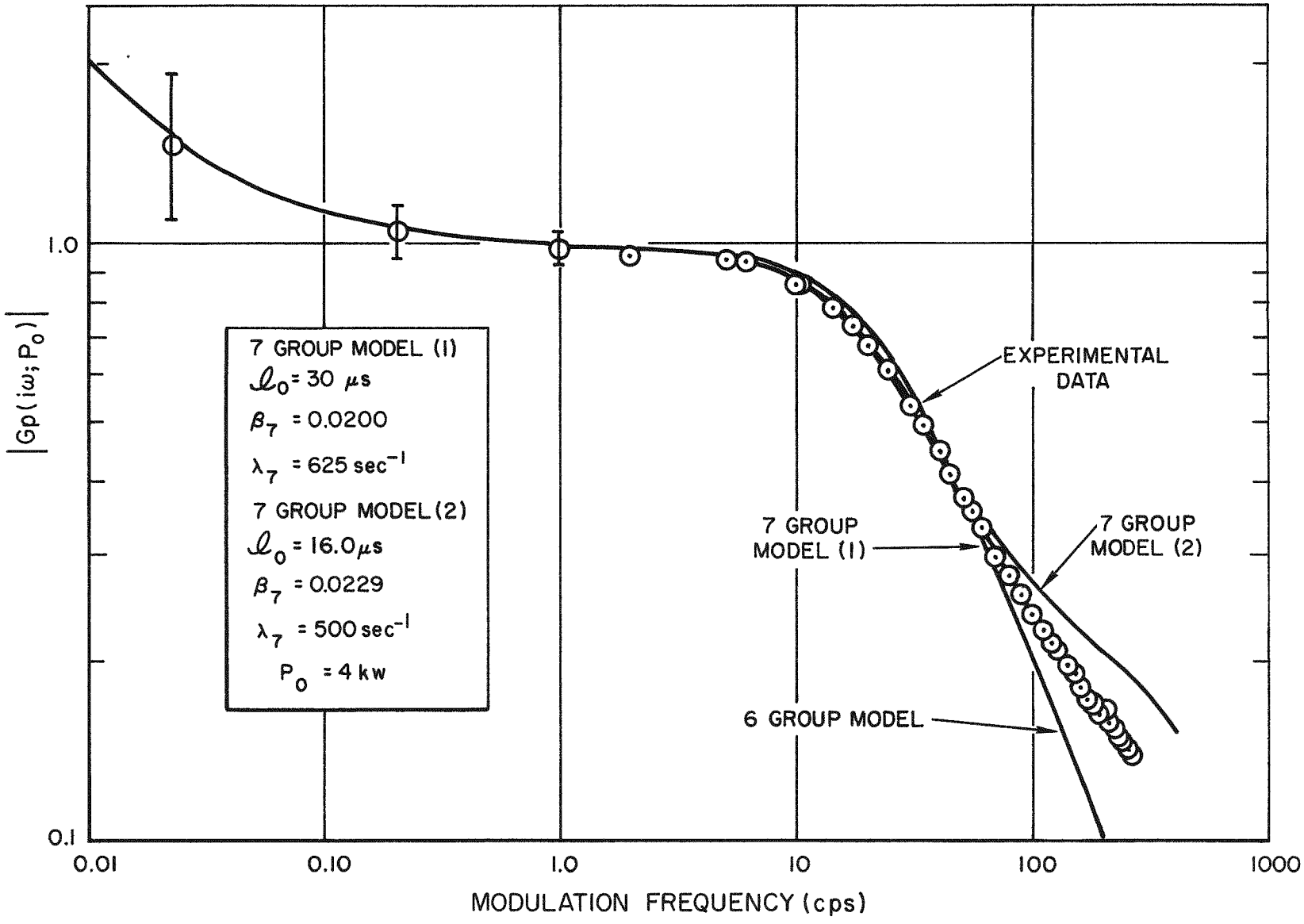

Figure 21. Comparisons with Theory - Amplitude

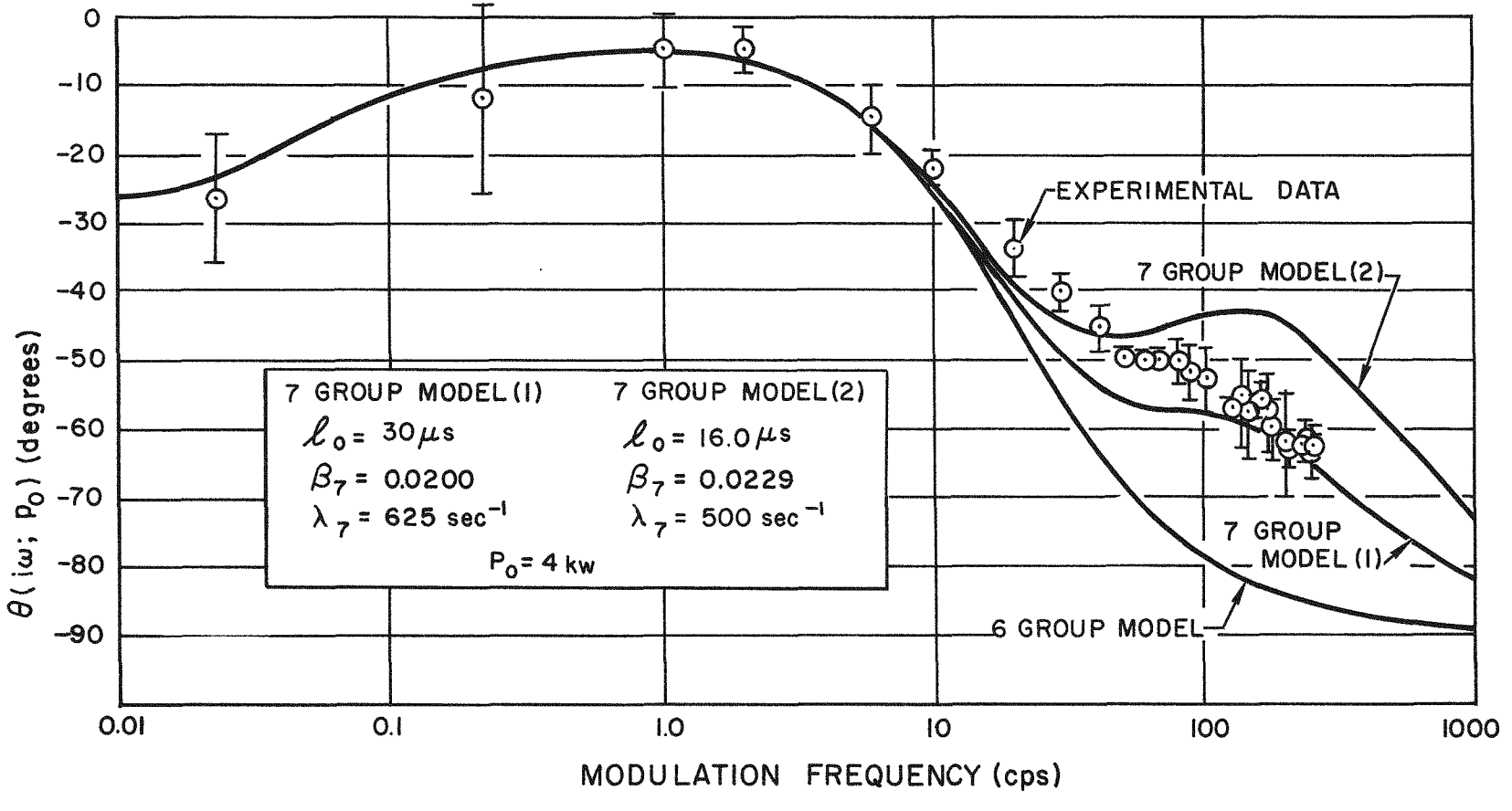

Figure 22. Comparisons with Theory - Phase

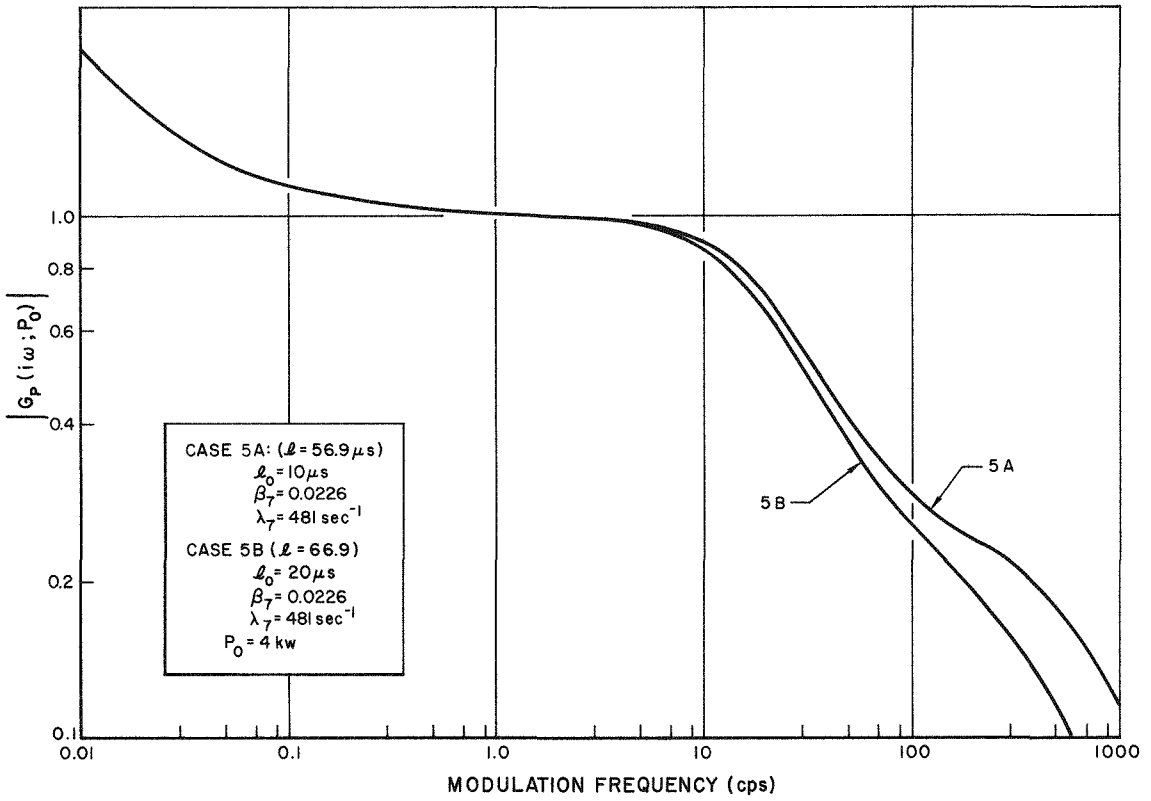

Figure 23. Effects of ℓ_0 on the Transfer Function - Amplitude

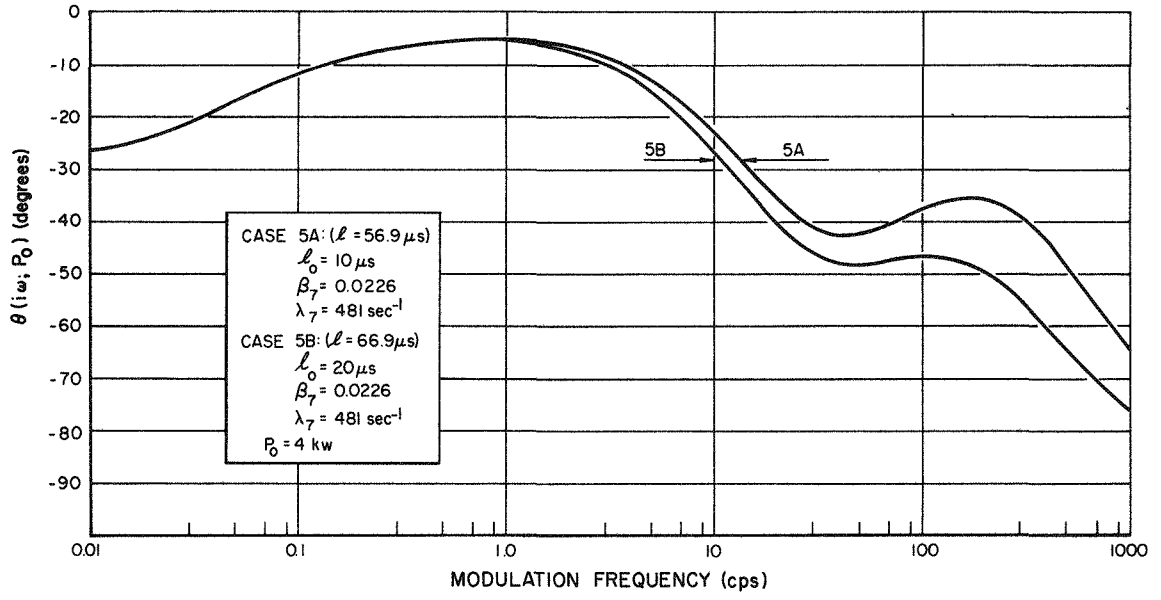

Figure 24. Effects of ℓ_0 on the Transfer Function - Phase

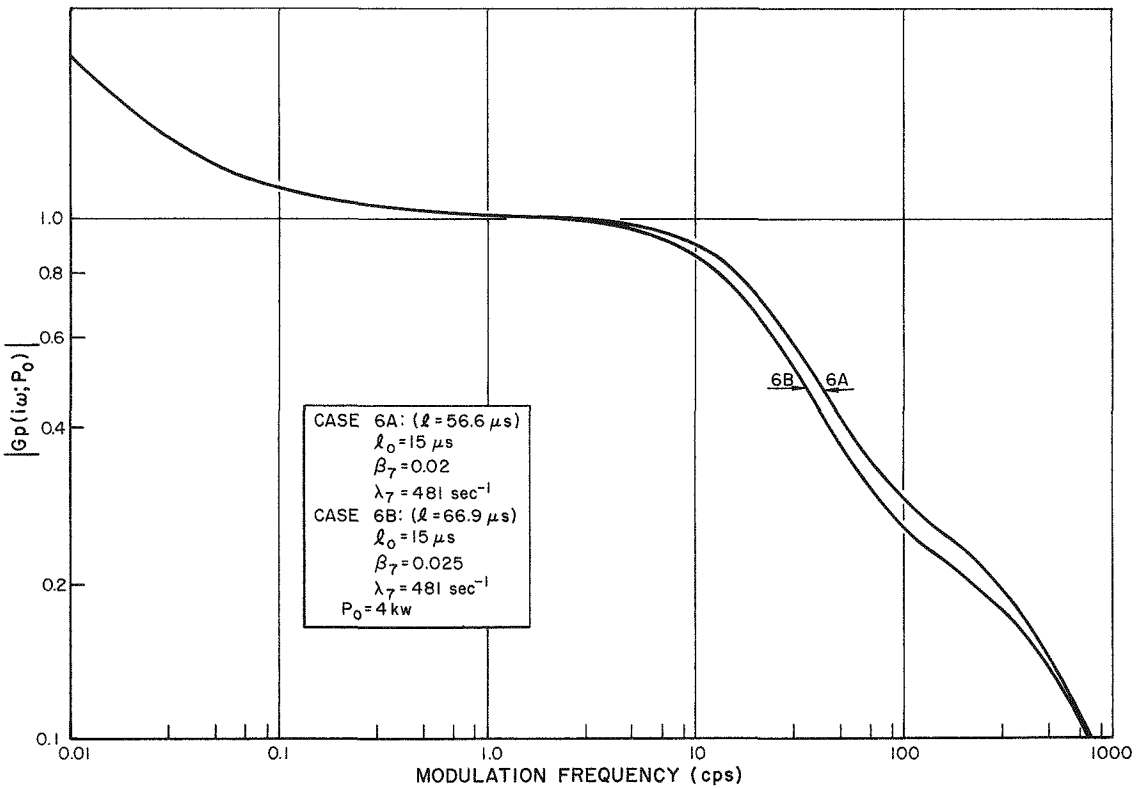

Figure 25. Effects of β_7 on the Transfer Function - Amplitude

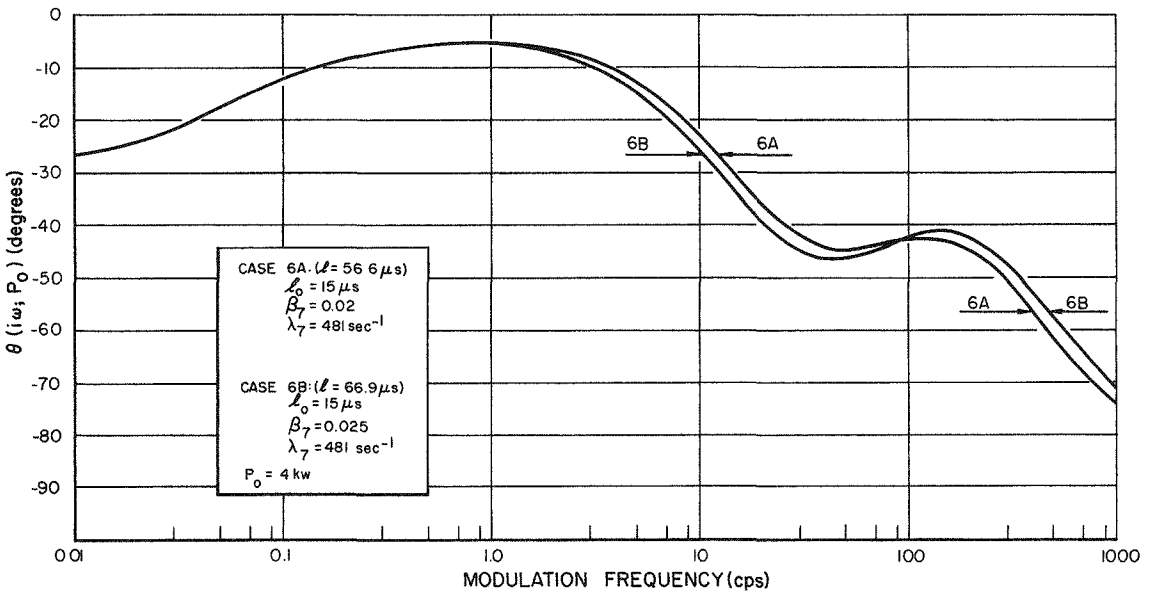

Figure 26. Effects of β_7 on the Transfer Function - Phase

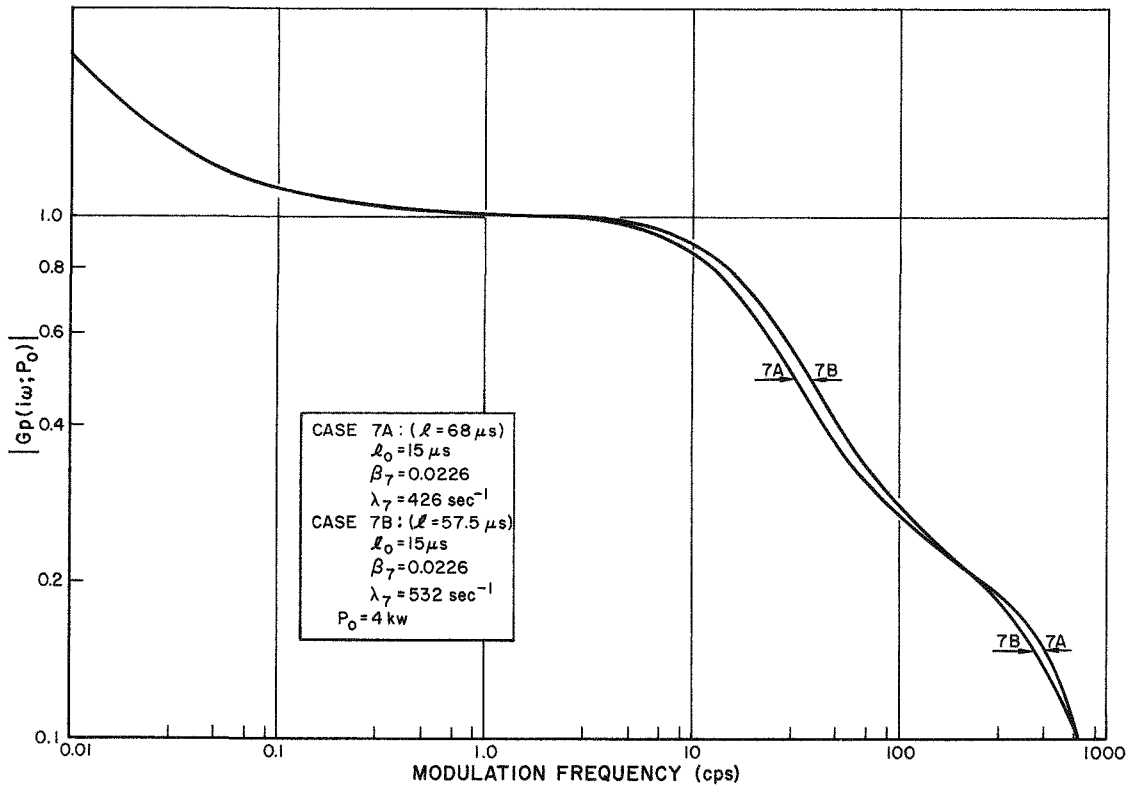

Figure 27. Effects of λ_7 on the Transfer Function - Amplitude

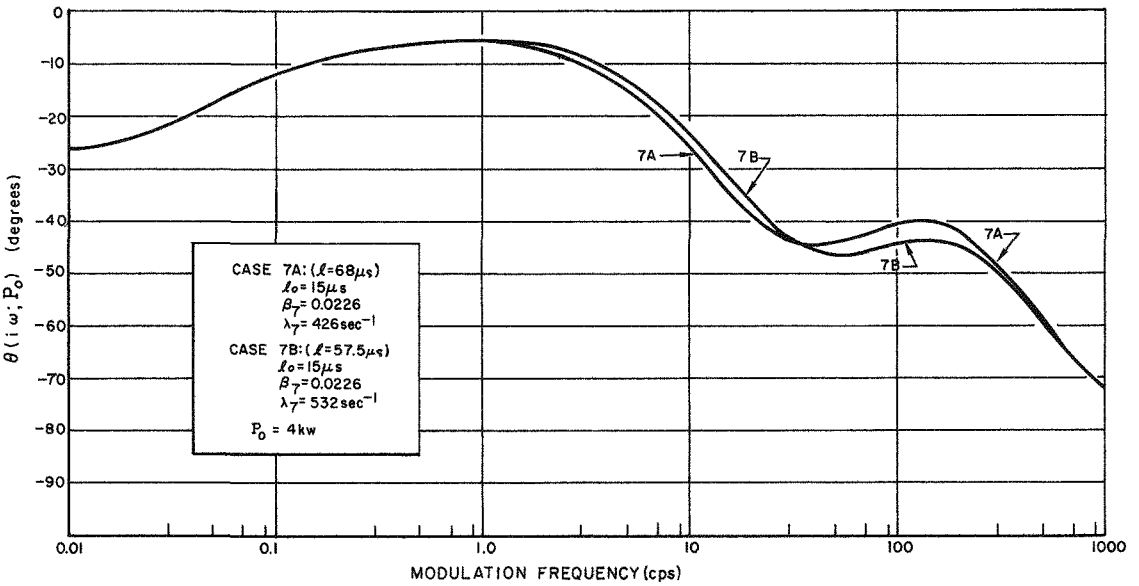

Figure 28. Effects of λ_7 on the Transfer Function - Phase

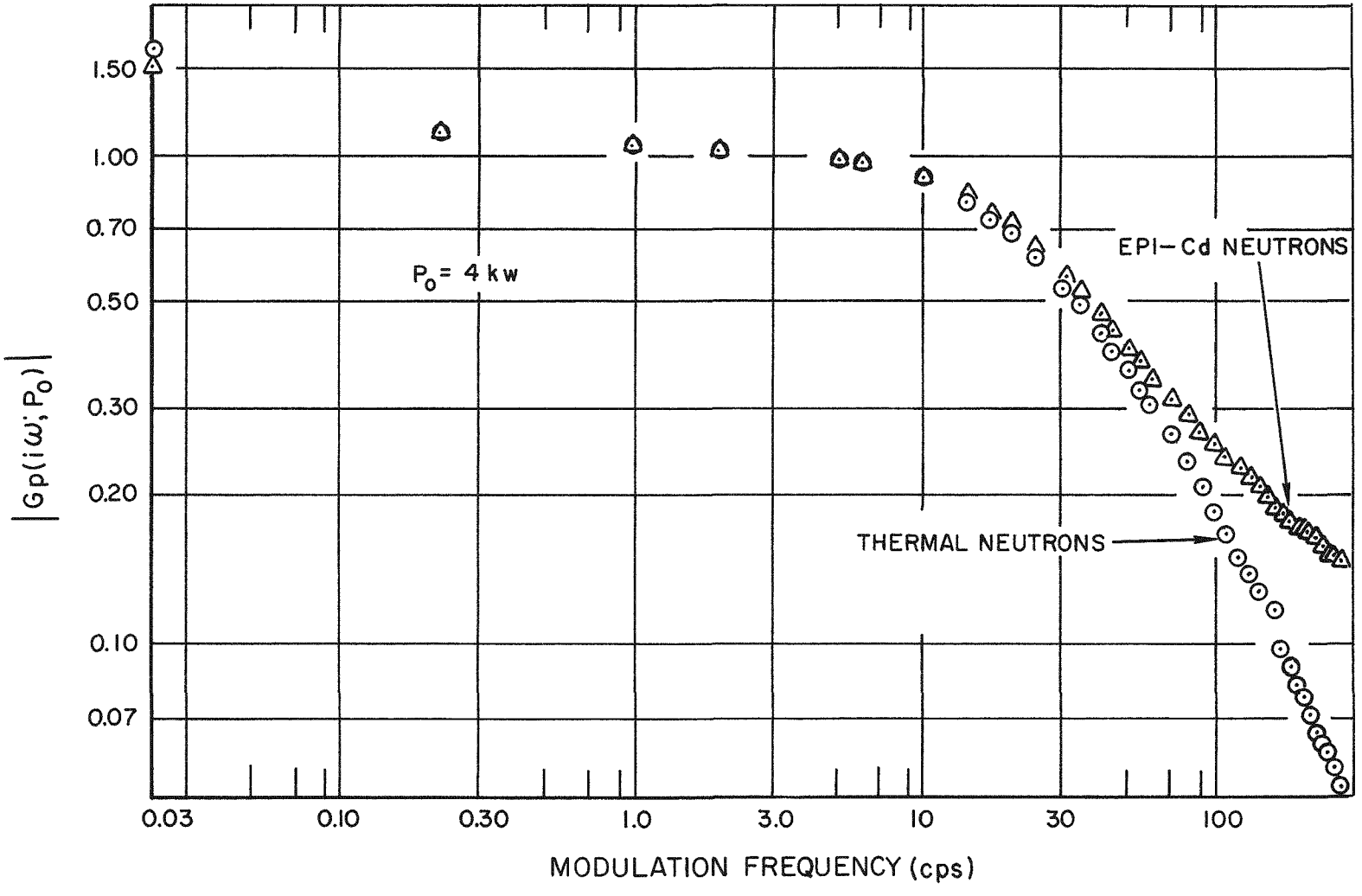

Figure 29. Diffusion Effects on the Transfer Function - Amplitude

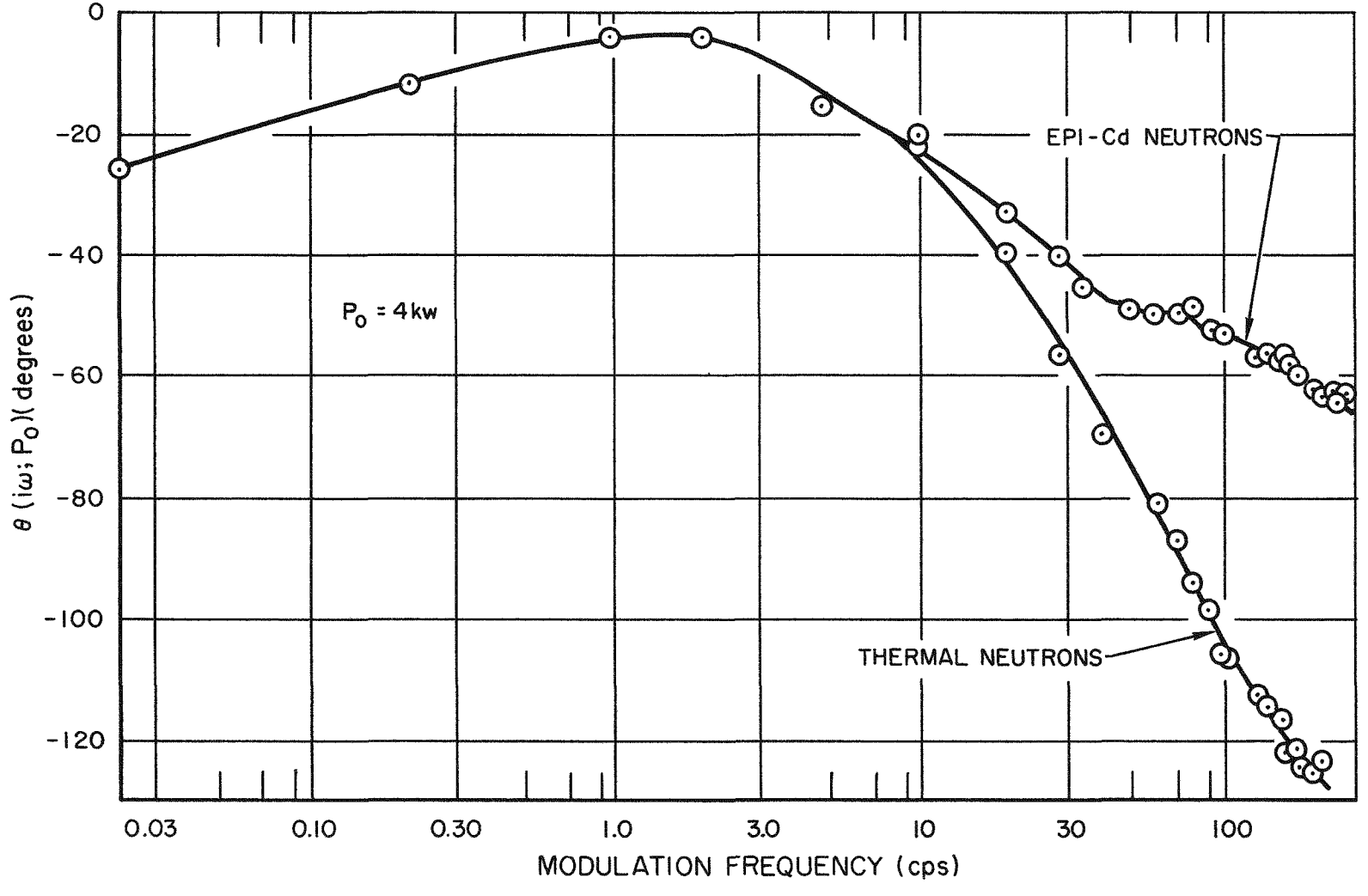

Figure 30. Diffusion Effects on the Transfer Function - Phase

VII. CONCLUSION AND RECOMMENDATIONS

An inspection of Figures 21 and 22 clearly indicates that the KEWB reactor does, in fact, operate in a manner that is more accurately described by a model incorporating as a separate group the reflector delayed neutrons rather than the conventional six group model. The constants of this seventh group cannot be determined precisely from the results reported here due to the transfer function's lack of sensitivity to small changes in their values. The possible error in the experimental values presented must be expanded in view of the fact that the data are based on epi-cadmium neutrons. The effects of diffusion to epi-cadmium energies may not be negligible. If not, correction would provide closer correlation with the theoretical values represented in Model 2.

The amplitude data do, however, permit a determination of the neutron lifetime, valid for slow transients, as 61.8 ± 2.4 μsec for an effective fraction of delayed neutrons of 0.008. This lifetime is computed at the break frequency of the reactor and the limits set by the Student's "t" test for 95% confidence. This value of lifetime compares with the value of 62.5 μsec as determined from the experimental inhour equation[2] and the value of 78.0 ± 3.0 μsec as determined by noise analysis.[12]

This experiment indicates no serious problems associated with amplitude and phase measurements at frequencies less than 50 cps. The measurement techniques do, however, need improvement at greater perturbation frequencies.

The following is a list of recommendations for such an improvement.

a) A brief check of the rod calibration should be made with the modulator installed, to more accurately determine the magnitude of the input reactivity.

b) The magnitude of the input reactivity, at the high perturbation frequencies, should be increased to improve the signal-to-noise ratio.

c) The reactivity waveform should be determined at each reactivity used.

d) The waveform of the input reactivity should be more accurately known. In addition to more data points, this would entail development of equipment that would indicate the rotor position in a direct manner. Errors due to timing and rotor acceleration (and deceleration) would then be eliminated.

e) The development of a high sensitivity, fast neutron detector would be a great advantage at these frequencies. In lieu of this, however, a refinement in the technique for determining the error contributed by epicadmium neutrons is required.

Should these improvements be achieved, one may find it possible to modulate to even greater frequencies and as a result obtain a greatly improved insight into the quantitative aspects of describing the KEWB reactor by seven groups of delayed neutrons.

NOMENCLATURE

$P(t)$ = total fission rate (or power) at time t, kw.

P_0 = reactor power (equilibrium level), kw.

$C_j(t)$ = power equivalent of the j^{th} group of delayed neutrons, kw.

$T(t)$ = instantaneous core temperature difference, at time t, from that at equilibrium power, °C.

$V(t)$ = instantaneous volume difference at STP, of radiolytic gas bubbles, at time t, from that at equilibrium power, cm^3.

$\rho(t)$ = $(k_{eff} - 1)/k_{eff}$, the reactivity in "absolute" units at time t, where k_{eff} is the effective multiplication factor.

$\rho_1(t)$ = the external input function of reactivity in absolute units.

ρ_0 = the magnitude of $\rho_1(t)$.

δP_1 = the magnitude of the power perturbation created by $\rho_1(t)$, kw.

ℓ = the effective neutron generation time in the reactor (assumed to have negligible time dependence), sec.

ℓ_0 = the effective generation time of neutrons which remain in the core, sec.

β = the effective total fraction of all neutrons which are delayed.

β_j = the effective fraction of all neutrons which belong to the j^{th} delayed group.

a_j = the effective fraction of all delayed neutrons which belong to the j^{th} delayed group, $\sum_{j=1}^{m} a_j = 1$.

λ_j = the representative decay constant of neutrons which belong to the j^{th} delayed group, sec^{-1}.

k_{ex} = excess multiplication factor.

G = the rate of radiolytic gas formation per unit power for the reactor, cm^3/kw-sec.

K = the reciprocal heat capacity for the reactor, °C/kw-sec.

σ = the reciprocal of the characteristic time for loss of radiolytic gas from the core, sec^{-1}.

γ = the reciprocal of the characteristic time for loss of heat from the core, sec^{-1}.

α = the temperature coefficient of reactivity in "absolute" units.

ϕ = the void coefficient of reactivity in "absolute" units.

$\rho^* = \rho/\beta$, the reactivity in dollars.

$\ell^* = \ell/\beta$.

$\alpha^* = \alpha/\beta$, the temperature coefficient of reactivity in dollars.

$\phi^* = \phi/\beta$, the void coefficient of reactivity in dollars.

ω = the perturbation frequency, radians/sec.

R = the preamp input resistance, ohms.

C = the total preamp input capacitance, f.

θ_{RC} = the phase error due to the RC time constant, degrees.

$|Z_1|$ = the amplitude of the transfer function evaluated at the fundamental frequency, ω.

$|Z_2|$ = the amplitude of the transfer function evaluated at the second harmonic frequency, 2ω.

θ_1 = the phase of the transfer function evaluated at the fundamental frequency, ω, degrees.

θ_2 = the phase of the transfer function evaluated at the second harmonic frequency, 2ω, degrees.

$\theta_{1,2} = \theta_1 + \theta_2$.

ξ = the average logarithmic energy decrement per collision of a neutron, dimensionless.

$\bar{\Sigma}_s$ = the average macroscopic scattering cross section, cm^{-1}.

m_0 = neutron mass, gm.

REFERENCES

1. R. E. Skinner and D. L. Hetrick, "The Transfer Function of a Water Boiler Reactor," Nuclear Science and Engineering 3, (May, 1958), p 573

2. Supplied by M. Dunenfeld, Atomics International, in a conversation with the author, 1959

3. R. E. Skinner, "Mean Life Times of Decay Constants for Latest Delayed Neutron Data, "NAA-TDR-2186 (October 7, 1957)

4. D. L. Hetrick and D. P. Gamble, "Transient Reactivity During Power Excursions in a Water Boiler Reactor,"1958 Winter Meeting of the American Nuclear Society (Detroit, Michigan, December 9, 1958)

5. L. G. Barrett, "Application of Pile Modulation Measurement Techniques," KAPL-M-LGB-13 (May 22, 1957)

6. A. M. Weinberg and E. P. Wigner, The Physical Theory of Neutron Chain Reactors (Chicago, University of Chicago Press, 1958)

7. C. A. Smith and M. Huntsinger, "A Low Cost Uncompensated Ionization Chamber for Monitoring Reactor Power," NAA-AER-MEMO-1437 (September 28, 1955)

8. Z. Akcasu, "General Solution of the Reactor Kinetic Equations Without Feedback," Nuclear Science and Engineering 3, (April, 1958), p 456

9. S. Glasstone, Principles of Nuclear Reactor Engineering (Princeton, New Jersey: D. Van Nostrand Company, Inc., 1955)

10. M. Huntsinger, "Ionization Chamber Response for KEWB Pile Oscillator Experiments," NAA-SR-MEMO-2295 (November 7, 1957)

11. M. Dunenfeld,"The Effect of Reflector-Moderated Neutrons on the Kinetics of the KEWB Reactor," Trans. Am. Nucl. Soc. 3 No. 1, (June, 1960) p 122

12. C. W. Griffin and J. G. Lundholm, Jr., "Measurement of the SRE and KEWB Prompt Neutron Lifetime Using Random Noise and Reactor Oscillation Techniques," NAA-SR-3765 (October 15, 1959)